WILEY

Carbon and Hydrogen

REVIEW OPEN ACCESS

Roadmap Toward the Production, Storage, Transportation, and Applications of Green Hydrogen

Xusheng Wang[1] | Xue Yang[2] | Xiang Wang[2] | Yingyan Zhao[1] | Xi Lin[1] | Zhigang Hu[1] | Guangqin Li[3] | Ruichang Xue[4] | Xinwei Guan[4] | Baowen Zhou[5] | Tianyi Ma[4] | Jianxin Zou[1,6]

[1]Shanghai Key Laboratory of Hydrogen Science & Center of Hydrogen Science, School of Materials Science and Engineering, Shanghai Jiao Tong University, Shanghai, China | [2]SINOPEC Research Institute of Petroleum Processing Co. Ltd, Beijing, China | [3]MOE Laboratory of Bioinorganic and Synthetic Chemistry, GBRCE for Functional Molecular Engineering, Lehn Institute of Functional Materials, School of Chemistry, Sun Yat-Sen University, Guangzhou, China | [4]Centre for Atomaterials and Nanomanufacturing (CAN), School of Science, RMIT University, Melbourne, Australia | [5]Key Laboratory for Power Machinery and Engineering of Ministry of Education, Research Center for Renewable Synthetic Fuel, School of Mechanical Engineering, Shanghai Jiao Tong University, Shanghai, China | [6]Department of Electrical Engineering, Cambridge Graphene Center, University of Cambridge, Cambridge, UK

Correspondence: Baowen Zhou (zhoubw@sjtu.edu.cn) | Tianyi Ma (tianyi.ma@rmit.edu.au) | Jianxin Zou (zoujx@sjtu.edu.cn)

Received: 4 September 2025 | **Revised:** 15 October 2025 | **Accepted:** 17 October 2025

Keywords: electrolysis | green hydrogen | photocatalysis | storage and transportation | utilization

ABSTRACT

Hydrogen, as a clean and versatile energy carrier, plays a vital role in the global transition toward carbon neutrality. Achieving a sustainable hydrogen economy requires safe, efficient, and cost-effective technologies across production, storage, transportation, and utilization. On the production side, electrolysis and solar-driven photocatalysis are rapidly advancing toward industrial adoption, yet remain constrained by electrolysis efficiency, cost, and electrolyzer durability. For storage and transportation, lowering costs and energy consumption, improving system efficiency, and deploying safe, high-capacity hydrogen storage and transportation solutions are key priorities. Regarding hydrogen utilization, particularly hydrogen fuel cells and hydrogen-based power systems, require further enhancement in their durability, reliability, and integration flexibility to enable widespread deployment across sectors. Therefore, this review provides a comprehensive overview of green hydrogen technologies, emphasizing recent advances, key challenges, and industrial demonstrations. By integrating insights from electrochemical and photochemical production, solid-state and liquid-phase storage, and hydrogen end-use pathways, we propose a roadmap toward the scalable deployment of green hydrogen infrastructure. Coordinated progress across these domains will position hydrogen as a cornerstone of a sustainable, secure, and decarbonized global energy solution.

1 | Introduction

Global energy-related carbon dioxide (CO_2) emissions increased by 0.8% in 2024, reaching a record high of 37.8 gigatons (GTs). This escalation has driven the atmospheric CO_2 concentration to an unprecedented level of 422.5 ppm, intensifying concerns over climate change and the urgency of transitioning to low-carbon energy systems [1]. Against this backdrop, hydrogen, as an environmentally friendly, abundant, and high-energy-density secondary energy source, is regarded as an ideal carrier for achieving the clean energy transition. With the advancement of hydrogen technologies and the improvement of upstream and downstream industrial chains, along with the introduction of efficient hydrogen storage technologies, electrolytic and photocatalytic hydrogen production powered by wind and solar resources has become a key technological pathway for large-scale renewable energy utilization.

Currently, the main electrolytic hydrogen production technologies include alkaline water electrolyzers (AWE) and proton exchange membrane electrolyzers (PEM), while anion exchange membrane electrolyzers (AEM) and solid oxide electrolysis cells

(SOEC) remain at earlier stages of technological development [2, 3]. Among them, AWE is the most mature technology on the market and is progressing toward large-scale and high-efficiency applications. Reports indicate that commercial AWE systems have already achieved current densities of over 9000 A m^{-3} and hydrogen production rates of 5000 Nm^3 h^{-1} [4]. PEM electrolysis offers flexible startup and can be integrated with AWE systems to enhance fast load response capabilities, while its widespread deployment remains constrained by high system and catalyst costs, as well as limited stack lifetimes in harsh operating environments [5]. In contrast, emerging AEM and SOEC technologies hold significant promise for long-term cost reduction and system performance enhancement, but are currently confined to laboratory-scale demonstrations and early-stage prototypes [6].

Because of hydrogen's inherently low volumetric energy density, high diffusivity and leakage tendency, wide flammability range, and the risk of hydrogen-induced embrittlement in certain metals, achieving safe, efficient, and large-scale hydrogen storage and transportation remains highly challenging [7, 8]. While hydrogen production and utilization projects have already exceeded the scale of tens of thousands of tons, current storage technologies remain limited to the scale of several hundred tons, severely constraining the large-scale development of hydrogen energy [9]. At present, high-pressure gaseous hydrogen is the most widely adopted storage method, typically transported using tube trailers at 20 MPa [10]. Although compressed gas storage technology is well established and offers high flexibility, it faces significant limitations in large-scale applications [11]. In addition to high-pressure storage, hydrogen can also be stored through liquefaction, physical adsorption, or chemical methods such as metal hydrides and liquid organic hydrogen carriers (LOHCs) [12]. Many emerging hydrogen storage and transport technologies are attracting growing attention from both the market and investors, due to their enhanced safety and higher hydrogen storage densities [13, 14]. Notably, in November 2024, Hydrexia (China) achieved a landmark breakthrough in large-scale, long-distance hydrogen transport with the shipment of the world's first large-scale magnesium-based solid-state hydrogen storage unit from Waigaoqiao Terminal to Malaysia. This milestone marks a major advancement in hydrogen export and infrastructure development [6].

Additionally, hydrogen functions as both an energy carrier and a chemical feedstock, which greatly broadens its scope of applications [15]. As an energy carrier, hydrogen can be used in a variety of sectors, including transportation and power generation. In the transportation sector, hydrogen fuel cells offer advantages such as long driving range, fast refueling, and zero emissions [16]. These characteristics make hydrogen especially suitable for heavy-duty trucks, buses, and rail transit, effectively overcoming the limitations of battery electric vehicles such as long charging durations and limited driving range. [17]. In power generation, hydrogen fuel cells or gas turbines can provide high-efficiency, flexible, and low-noise local power supply, making them ideal for scenarios requiring high energy security and autonomy, such as hospitals, data centers, and remote areas [18]. Within the chemical sector, hydrogen is commonly utilized for ammonia synthesis, petroleum refining, and steelmaking, serving as a vital reductant and feedstock in numerous key industrial processes [19].

The hydrogen energy sector spans production, storage, transportation, and utilization. Realizing its efficient and large-scale growth demands safe and effective implementation throughout the entire supply chain. Previous reviews have mostly focused on individual aspects of hydrogen energy, such as production, storage, or applications, while rarely providing a systematic overview from a full industry chain perspective. This limits comprehensive understanding of the overall development, technological bottlenecks, and future trends of hydrogen energy from production to end-use. Based on the above, this review focuses on analyzing the critical technologies, existing bottlenecks, and prospective advancements throughout the full green hydrogen supply chain. Although green hydrogen currently lacks cost competitiveness compared to gray hydrogen, ongoing improvements in electrolyzer efficiency and falling costs of renewable electricity are expected to enhance its economic viability. Simultaneously, breakthroughs in novel hydrogen storage and transportation technologies, such as metal hydride-based hydrogen storage and advanced green ammonia synthesis/decomposition approaches, could significantly lower energy expenses in the hydrogen supply processes. Furthermore, hydrogen fuel cell technology is also steadily maturing, enabling clean and efficient energy conversion. However, large-scale deployment in sectors like transportation and industry continues to face challenges, including the need to further reduce system and operating costs, develop comprehensive hydrogen refueling infrastructure, and enhance the durability and reliability of fuel cell stacks.

2 | Green Hydrogen Production Technologies

2.1 | Green Hydrogen Production via Electrolysis

Green hydrogen production via electrolysis represents a sustainable and environmentally benign approach, wherein water is split into hydrogen and oxygen using electricity from renewable sources like solar, wind, or hydropower. This process relies on an electrolyzer, often using proton exchange membrane or alkaline technologies, to drive the reaction. Unlike conventional hydrogen production from fossil fuels, water electrolysis generates no CO_2 emissions, offering a zero-carbon alternative. Green hydrogen holds substantial potential across sectors such as clean energy storage, transportation, heavy industry, and heating. Moreover, it also helps balance intermittent renewable power by storing surplus electricity as hydrogen. Therefore, green hydrogen is regarded as a key solution for building a carbon-neutral energy system and achieving long-term climate and energy security targets.

Table 1 compares the performance, advantages, and disadvantages of the main water electrolysis technologies [20–24], including alkaline (ALK), proton exchange membrane (PEM), anion exchange membrane (AEM), and solid oxide electrolysis (SOE) systems. Currently, ALK electrolysis remains the most widely adopted and mature hydrogen production technology. However, its efficiency is relatively low, and the leakage of alkaline electrolytes can cause environmental issues. In contrast, PEM and SOE represent next-generation electrolysis technologies. PEM electrolysis offers a fast dynamic response, while SOE shows high electrolysis efficiency. Nevertheless, both are facing certain limitations: PEM relies on expensive noble

TABLE 1 | Comparison of different electrolysis technologies [20–24].

Specification	ALK	PEM	AEM	SOE
Working fluid	Liquid	Distilled water	Distilled water or low concentration solution	Steam
Operating temperature (°C)	60–80	50–80	50–60	500–850
Operating pressure (bar)	1–30	1–70	1–30	1–25
Average current density (A/cm^2)	0.2–0.6	0.6–2	0.1–0.5	0.3–1
Efficiency	59%–70%	65%–82%	—	80%–90%
Stack lifetime (h)	6000–80,000	8000–60,000	—	20, 000
Cost ($/kWh)	500–1400	1100–1800	—	2800–5600
Advantages	Low cost, relative stable, mature technology	Fast response/start-up, high-purity H_2	Combines the advantages of ALK and PEM	High efficiency, low cost of catalyst
Challenges	Low efficiency, alkali leakage issues	High cost, precious metal catalyst	Poor stability, low hydroxide ion conduction	Slow response, mechanically unstable electrodes

metal catalysts, whereas SOE, due to its high operating temperature and significant thermal inertia, exhibits poor dynamic regulation capability. At present, the use of electrolysis technologies in renewable energy power generation has become relatively mature. For example, the Xinjiang Kuqa green hydrogen energy project, which commenced its operation in July 2023, achieved an annual production of 20,000 t of green hydrogen by using solar power for water electrolysis [25]. In addition, hybrid ALK-PEM electrolysis systems show great potential. Specifically, ALK electrolysis is cost-effective but has a slow dynamic response, whereas PEM electrolysis features a fast response but is more expensive. By integrating the two, the system can achieve high reliability in wind and solar power generation, thereby reducing renewable energy curtailment [26]. Furthermore, Wang et al. reported an integrated SOEC-photovoltaic system that utilizes magnesium-based solid-state hydrogen storage. The optimization of fins and heat transfer structures within the metal hydride bed was found to enhance the SOEC's electrical efficiency by 5%–9.3% [9].

2.1.1 | Alkaline Electrolysis

Alkaline water electrolysis hydrogen production systems have the advantages of mature technology, low cost, and easy maintenance, making them widely used in commercial applications. For example, the Xinjiang Kuqa Green Hydrogen Demonstration Project, operated by Sinopec in 2022, is equipped with an alkaline water electrolysis system with a capacity of approximately 240 MW and achieved an output of 20,000 tons per year of green hydrogen by using solarvotalic power to electrolyze water [25]. In 2024, Shuangliang Group released its self-developed alkaline water electrolyzer with a capacity of 5000 $Nm^3\ h^{-1}$. The electrolyzer can achieve a maximum current density of up to 10,600 A m^{-2} with an energy consumption of 4.7 $kWh{\cdot}Nm^3$ H_2 [4]. Additionally, the minimum operational load of the electrolyzer can be reduced to 10%, while maintaining an oxygen content in the hydrogen of less than 1.50% at this load. These demonstration projects prove that alkaline water electrolysis technology is moving toward high production rate and low-cost solutions, making it a leading candidate for efficient green hydrogen production from renewable energy.

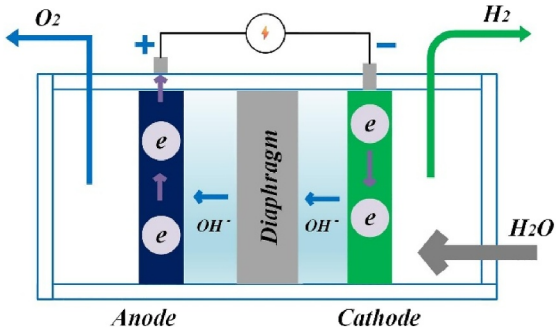

FIGURE 1 | The schematic of the alkaline electrolyzer.

The alkaline water electrolysis hydrogen production system mainly consists of the electrolyzer and a separation layer. The typical structure of an alkaline electrolyzer is shown in Figure 1. During the water electrolysis process, the cathode undergoes a reduction reaction, breaking down water into hydrogen gas and hydroxide ions (OH^-). Meanwhile, at the anode side, an oxidation reaction converts OH^- into oxygen gas and water. The membrane (diaphragm) plays a crucial role in facilitating the transport of water and hydroxide ions while simultaneously separating the gases to prevent the mixing of hydrogen and oxygen. The anodic, cathodic, and overall reactions in alkaline electrolysis are presented below [27]:

$$\text{Cathode reaction}: \quad 2H_2O + 2e^- \rightarrow H_2 + 2\,OH^- \tag{1}$$

$$\text{Anode reaction}: \quad 2\,OH^- \rightarrow \frac{1}{2}O_2 + H_2O + 2e^- \tag{2}$$

$$\text{Overall reaction}: \quad H_2O\,(l) \rightarrow H_2 + \frac{1}{2}O_2 \tag{3}$$

In an alkaline electrolyzer, the anode material must exhibit excellent electrocatalytic performance. Common anode materials include nickel and its alloys, such as nickel-iron (Ni-Fe) and nickel-cobalt (Ni-Co) alloys [28], which enhance oxygen evolution reaction (OER) activity. For the cathode, high electrical conductivity, stability, and durability in an alkaline environment are essential. Common cathode materials include nickel and stainless steel, often further modified with catalysts such as nickel-molybdenum (Ni-Mo) or nickel-tungsten (Ni-W) alloys to improve hydrogen evolution reaction (HER) efficiency and reduce overpotential [29]. The membrane in an alkaline electrolyzer serves to separate hydrogen and oxygen gases while allowing ion transport. However, its relatively low ionic conductivity and irreversible degradation at relatively high temperatures limit both the electrolysis efficiency and the operating temperature of the electrolyzer. Common membrane materials include ionic conductive polymer membranes, alkaline-stable polymer membranes, composite membranes, and gel electrolyte membranes, each offering different balances of conductivity, stability, and durability to improve overall system performance [29]. Additionally, NaOH or KOH (20–30 wt%) is commonly used as the electrolyte solution in alkaline water electrolysis, providing high ionic conductivity and ensuring efficient ion transport between electrodes [30].

Although alkaline water electrolysis hydrogen production systems offer good economic benefits, they still face several technical challenges, including low hydrogen production efficiency, long startup times, and limited operational flexibility [31]. The future development of electrocatalysts for alkaline water electrolysis will focus on the development of low-cost, nonprecious metal catalysts, such as transition metals (nickel, cobalt, iron, etc.) and their compounds [32]. In addition, designing catalysts with precisely controlled structures (e.g., single-atom catalysts, two-dimensional materials, porous frameworks, and core-shell structures) can significantly improve catalytic efficiency and selectivity, reduce overpotential, and optimize electrochemical reaction pathways. For instance, Wang et al. synthesized Ni_3N nanoparticles through the controlled nitridation of Ni-based coordination polymer nanosheets [33]. By weakening the hydrogen binding energy of the nickel-based catalyst, they achieved enhanced catalytic activity. The preparation process is illustrated in Figure 2a. Figure 2b presents the HER performance of the developed catalyst in 1 M KOH. The results demonstrate that the np-Ni_3N exhibits excellent HER stability and achieves an activity comparable to that of the Pt benchmark. Although noble metal catalysts lack cost competitiveness in large-scale electrolytic hydrogen systems, their exceptional performance remains crucial for laboratory-scale or small-capacity electrolysis systems [35]. Moreover, the addition of a small amount of noble metal catalysts to the electrode material can provide satisfactory economic benefits during long-term operation. Zuo et al. proposed that incorporating a minimal amount of Ru in cathodes (~0.04 g_{Ru} per kW) is a promising strategy to balance the capital and operational expenditures of conventional alkaline electrolyzers for high-throughput operation. As shown in Figure 2d, their system operated in a 30 wt% KOH aqueous solution at 80°C under atmospheric pressure (~1 bar), demonstrating stable performance over 1000 h at a current density of 1 A cm^{-2}, as presented in Figure 2c [34].

2.1.2 | Proton Exchange Membrane Electrolysis

Proton exchange membrane water electrolysis (PEMWE) is a key technology for industrial hydrogen production, offering distinct advantages in applications requiring high-purity hydrogen and rapid response, such as renewable energy grid integration and distributed hydrogen energy systems [36]. Thanks to its capability for rapid start-up and high-efficiency operation at high current densities and low overpotentials, PEMWE has achieved substantial commercial advancements over the past decade [37]. Notable examples include Europe's HyBalance (1.2 MW, wind-powered), Japan's FH2R (20 MW, solar-powered) [38], and a U.S. California station using off-peak grid power for hydrogen fuel cell vehicles [39].

The core of proton exchange membrane (PEM) water electrolysis lies in the synergistic interaction between the proton exchange membrane and electrodes. As illustrated in Figure 3, a typical PEMWE system comprises a proton exchange membrane (PEM), a catalyst layer (CL), a gas diffusion layer (GDL), a bipolar plate (BPP), and other auxiliary components. During electrolysis, water molecules are oxidized at the anode, producing oxygen gas, protons (H^+), and electrons. The reaction can be represented as:

$$H_2O \rightarrow \frac{1}{2}O_2 + 2H^+ + 2e^- \quad (4)$$

The generated protons migrate through the proton exchange membrane to the cathode while the electrons travel through an external circuit, providing the necessary electrical energy to drive the reaction. At the cathode, the protons recombine with electrons to form hydrogen gas, following the reaction:

$$2H^+ + 2e^- \rightarrow H_2 \quad (5)$$

Owing to the underlying proton transport mechanism, PEMWE systems inherently operate in an acidic environment. In this configuration, the proton exchange membrane plays a dual role: it serves as both a separator preventing gas crossover and a conductor facilitating proton transfer, thereby ensuring the high purity of the produced hydrogen and oxygen [40]. Compared with other techniques, PEMWE exhibits several advantages, such as rapid response, high current density, and superior efficiency, which have collectively made it a focal point of research and industrial application. In the meantime, the development of highly active and stable electrocatalysts is critical to reducing the cost of PEMWE and facilitating industry applications [41]. In line with these technological merits, the U.S. Department of Energy (DOE) has set an ambitious technical goal: by 2026, achieving a hydrogen production cost of 2 \$ kgH_2^{-1}, with a long-term goal of 1 \$ kgH_2^{-1} by 2031. Additionally, the operational lifespan of PEMWE systems is targeted to increase from the current 40,000 h to 80,000 h by 2026 [42]. To advance the PEMWE technique, current research primarily focuses on electrode catalysts, proton exchange membranes, and bipolar plates. The key objectives are to develop novel catalysts and membranes with enhanced catalytic performance and durability while simultaneously reducing the overall cost of PEMWE systems.

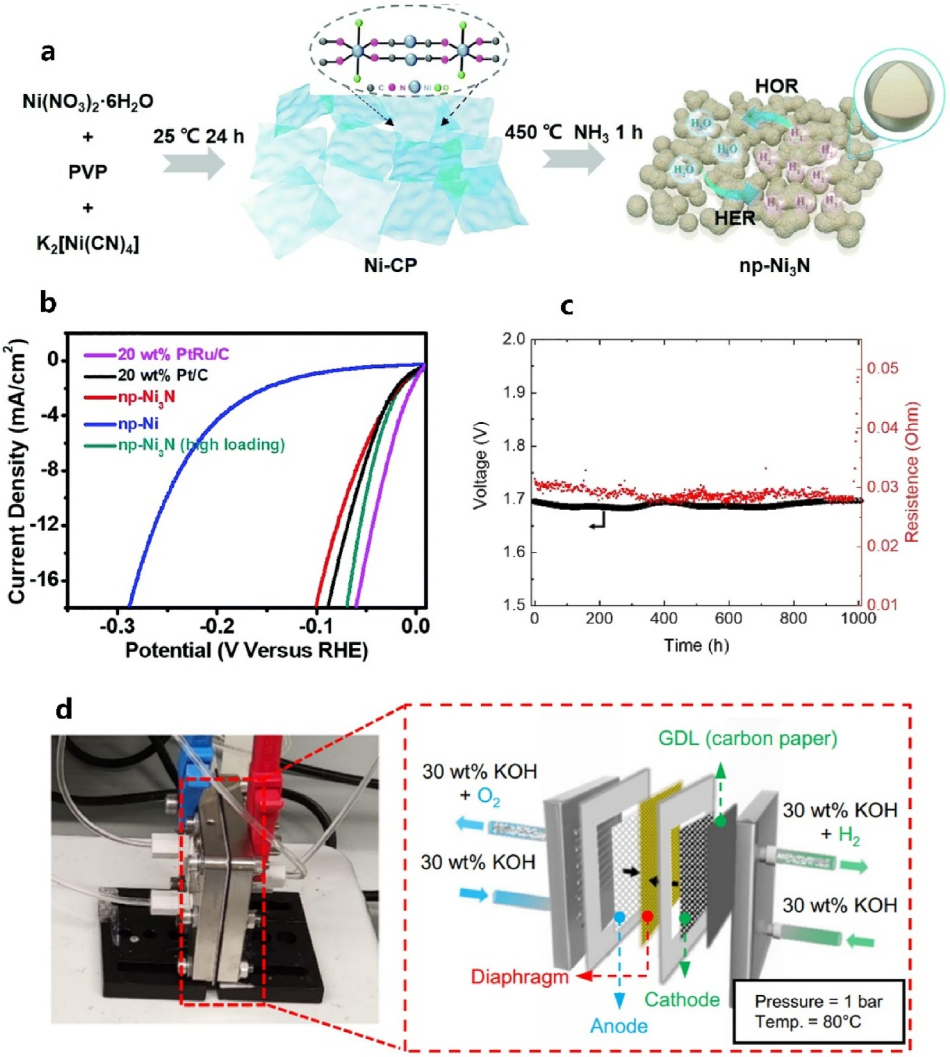

FIGURE 2 | (a) Schematic synthetic procedure toward np-Ni_3N. (b) HER polarization curves of np-Ni, np-Ni_3N, 20 wt% Pt/C and 20 wt% PtRu/C in 1 M KOH, Reproduced with permission [33], Copyright 2019, Royal Society of Chemistry. (c) Continuous stability test for AELs at 1 A cm^{-2} for 1000 h. (d) Set-up and sketch of the AELs configuration, Reproduced with permission [34], Copyright 2025, Springer Nature.

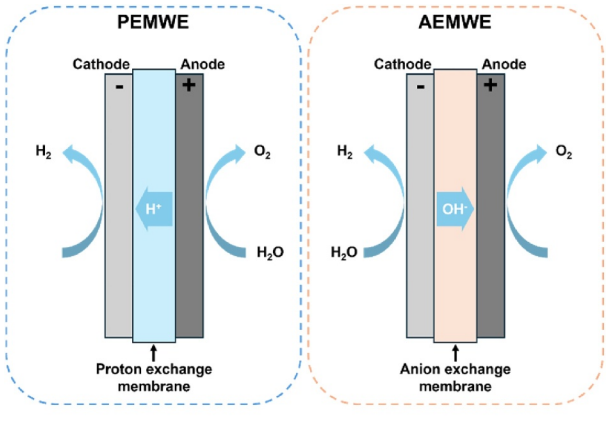

FIGURE 3 | The schematic diagram of PEMWE and AEMWE.

A central challenge in PEMWE technology is the development of robust catalysts capable of withstanding the oxidative and acidic operating environment. In such conditions, catalyst materials are prone to degradation, which has traditionally necessitated the use of high-cost noble metals such as iridium (Ir) and platinum (Pt) to ensure both stability and high catalytic performance. The high cost and scarcity of these materials have motivated extensive research into reducing noble metal usage while maintaining catalytic efficiency [43]. One effective strategy involves constructing heterojunctions with nonprecious functional materials. In this context, Wang et al. developed a novel IrO_2-based nanocatalyst with a tri-layered architecture, denoted as IrO_2@TaO_x@TaB [44]. This structure consists of ultrasmall IrO_2 nanoparticles anchored onto an amorphous TaO_x overlayer supported on the conductive TaB nanorod substrate (Figure 4a,b). The unique dual-interface structural design significantly enhances the catalyst's activity and stability for the OER in acidic environments, with the TaO_x layer facilitating electron transfer to IrO_2, thereby tuning the Ir^{3+}/Ir^{4+} ratio and accelerating OER kinetics. As a result, a low-Ir-loading (0.26 mgIr cm^{-2}) PEMWE system incorporating this catalyst achieves exceptionally high current densities at low cell voltages (e.g., 3.9 A cm^{-2} at 2.0 V, Figure 4c) and maintains stable performance for over 1500 h at a current density of 2.0 A cm^{-2} (Figure 4d).

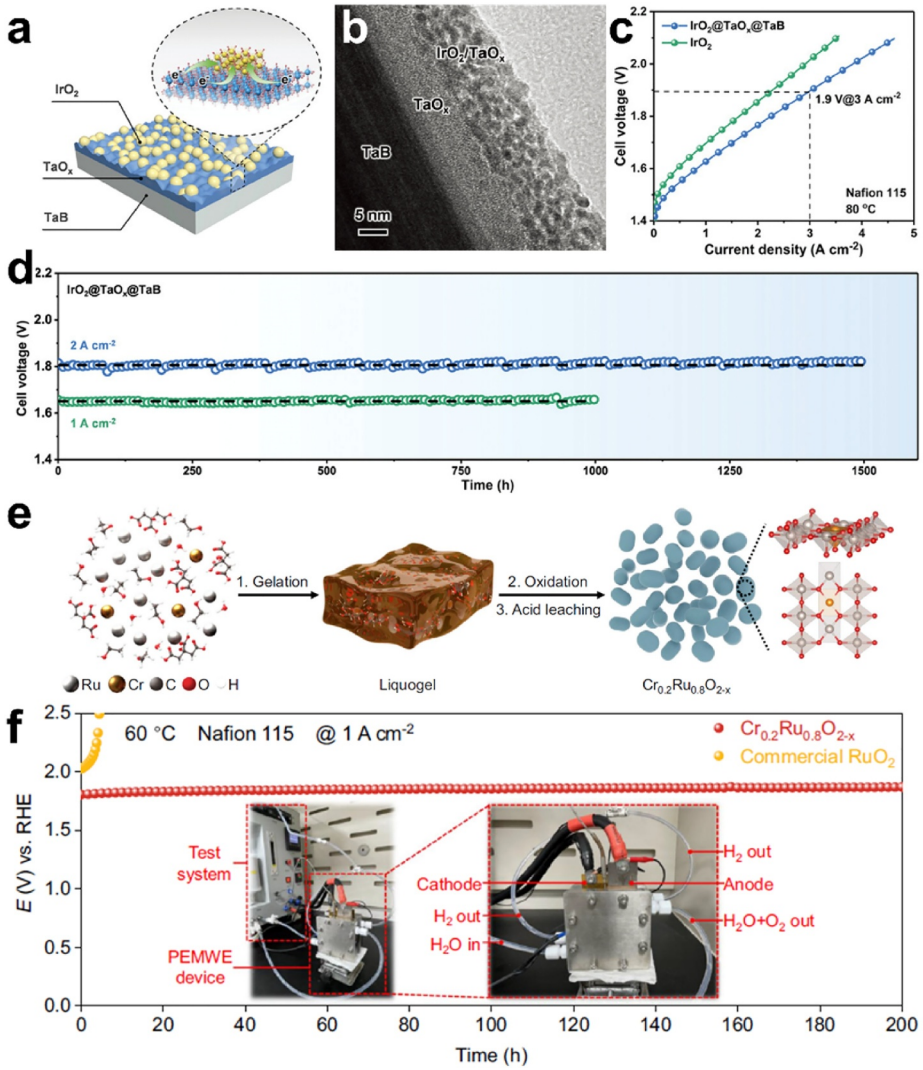

FIGURE 4 | (a) Schematic illustration of the interfacial electronic interactions in the IrO_2@TaO_x@TaB composite. (b) TEM image of the IrO_2@TaO_x@TaB electrocatalyst. (c) Polarization curves of PEMWEs using IrO_2@TaO_x@TaB and IrO_2 anodes, measured at 80°C with a Nafion 115 membrane. (d) Chronopotentiometry curves of PEMWEs employing the IrO_2@TaO_x@TaB anode under current densities of 1.0 and 2.0 A cm^{-2}, Reproduced with permission [44], Copyright 2024, Wiley. (e) Schematic representation of the synthesis process of $Cr_{0.2}Ru_{0.8}O_{2-x}$. (f) Chronopotentiometry curves of the PEMWE device using $Cr_{0.2}Ru_{0.8}O_{2-x}$ and commercial RuO_2 as anode catalysts, recorded at 1 A cm^{-2} and 60°C. The insets display photographs of the PEMWE device, Reproduced with permission [45], Copyright 2024, Springer Nature.

In addition to heterojunction engineering, doping with non-precious metals is another effective approach to reducing noble metal dependence while imparting multiple beneficial effects. In a recent representative study, Shen et al. reported a chromium-doped ruthenium dioxide ($Cr_{0.2}Ru_{0.8}O_{2-x}$) catalyst featuring oxygen vacancies (Figure 4e) [45]. Both experimental and theoretical studies revealed that Cr doping and oxygen vacancies introduce a dopant-mediated hydroxyl spillover mechanism, where hydroxyl species (OH*) adsorbed on Cr sites transfer to adjacent Ru active sites, accelerating the formation of OOH* intermediates and thus boosting catalytic efficiency. Additionally, the synergy between Cr dopants stabilizes both surface Ru and lattice oxygen, enhancing the long-term structural integrity of the catalyst. When employed as the anode catalyst in a practical PEMWE system, $Cr_{0.2}Ru_{0.8}O_{2-x}$ exhibited excellent long-term durability, maintaining stable operation for over 200 h at an ampere-level current density under 60°C (Figure 4f).

PEMWE is a highly promising technology for sustainable hydrogen production. Through the continuous exploration and innovation of catalyst design, researchers are making significant advancements in reducing noble metal usage while enhancing catalytic performance. In addition, optimizing high-performance polymer membranes, along with advancing system integration and scale-up engineering, should be prioritized. As these efforts progress, the cost of hydrogen production will continue to decrease, accelerating the realization of a green-hydrogen economy.

2.1.3 | Anion-Exchange Membrane Electrolysis

Anion exchange membrane water electrolysis (AEMWE) is another pivotal technology in the field of water electrolysis for hydrogen production. Unlike the PEMWE, which operates in an acidic environment, AEMWE utilizes an anion exchange

membrane to separate the generated hydrogen and oxygen gases, and the system typically operates under alkaline conditions. This significantly reduces the reliance on precious metal catalysts and corrosion-resistant metal components, positioning AEMWE as a promising candidate for low-cost green hydrogen production. Compared to traditional alkaline electrolyzers, AEMWE can operate without free alkaline solutions or in low-concentration alkaline environments while maintaining high ionic conductivity and simplifying system sealing and safety requirements. In recent years, with continuous advancements in AEM materials and alkaline stability, several small- to medium-scale demonstration projects have been deployed, such as the AEM Electrolyzer from Evebattery [46] and Enapter [47], integrating AEM electrolysis systems with renewable energy sources and distributed hydrogen production scenarios.

The working mechanism of AEMWE is similar to that of PEMWE, except that hydroxide ions are the primary charge carriers instead of protons. At the cathode, water molecules gain electrons to produce hydroxide ions (OH^-) and hydrogen gas through the reaction:

$$2H_2O + 2e^- \rightarrow H_2 + 2OH^- \quad (6)$$

The generated OH^- then migrate through the anion exchange membrane to the anode side, where they are oxidized to produce oxygen gas, water, and electrons via the reaction:

$$2OH^- \rightarrow \frac{1}{2}O_2 + H_2O + 2e^- \quad (7)$$

These electrons are then transported back to the cathode to complete the circuit [48]. A schematic illustration (Figure 5a) depicts the internal structure and ion transport pathways of AEMWE. Compared to PEMWE, AEMWE offers advantages such as lower cost and high hydrogen production efficiency, because of its nonprecious materials application. Despite its potential, AEMWE is still in an early stage of development compared to PEMWE. In particular, the sluggish kinetics of the OER remain a primary challenge, significantly limiting the overall efficiency of AEMWE systems.

The development of highly efficient, cost-effective, and stable nonprecious metal OER electrocatalysts is essential for achieving large-scale industrial applications and ensuring the commercial viability of AEMWE technology. Significant progress has been made in this area, with various transition metal-based catalysts, including oxides, (oxy)hydroxides, layered double hydroxides (LDHs), sulfides, phosphides, and molecular complexes. Among these, NiFe-LDHs have been identified as one of the most promising OER catalysts due to their low cost and unique microstructure [49]. For instance, Sun's group recently developed a nickel-iron-based electrocatalyst (CAPist-L1) using a one-step seed-assisted heterogeneous nucleation method (Figure 5a) [49]. In this process, insoluble nanoparticles in the heterogeneous nucleation system facilitate the formation of a dense interlayer, which effectively anchors the catalyst material onto the substrate, thereby enhancing stability and durability. As a result, the CAPist-L1 catalyst demonstrated an exceptional operational lifespan of 15,200 h (over 21 months) at a current density of 1000 mA cm^{-2} in 1 M KOH. When employed as the anode catalyst in an actual AEMWE device (25 cm^2), CAPist-L1 achieved a current density of 2730 mA cm^{-2} at 1.80 V and 60°C, surpassing the U.S. Department of Energy's hydrogen production target (1.80 V at 2000 mA cm^{-2}, Figure 5b). Furthermore, the catalyst exhibited high electrolysis performance under high current densities (7350 mA cm^{-2} for a 1 cm^2 electrolyzer at 2.0 V and 80°C) and outstanding stability (1500 h for both 1 and 25 cm^2 electrolyzers at 1000 mA cm^{-2}, Figure 5c). These promising results underscore the potential of AEMWE for large-scale applications, although further research is required to optimize catalyst performance and lower overall costs.

In addition to catalysts, the anion exchange membrane (AEM) plays a vital role in the advancement of AEMWE technology. AEMs are primarily composed of a polymer backbone with attached cationic functional groups, which govern their ion transport properties. Extensive research has been conducted to develop high-performance AEMs using various polymer backbones, including poly (arylene ether), poly(norbornene), poly (benzimidazole), and ether-free polyarylenes. Moreover, a diverse range of cationic functional groups, such as quaternary ammonium, imidazolium, phosphonium, and metallocene derivatives, have been explored to enhance ionic conductivity, chemical stability, and overall performance. In 2024, Yin et al. reported a series of branched poly(aryl-quinuclidinium) (PAQ-x) AEMs, synthesized using a 1-methyl-3,3-diphenylquinuclidinium molecular building unit and processed via acid-catalyzed Friedel–Crafts polymerization (Figure 5d,e) [50]. These PAQ-x AEMs feature controllable molecular weights and adjustable ion exchange capacities, enabling excellent electrochemical performance. The optimized AEM achieved a current density of 8 A cm^{-2} at 2.0 V and 80°C, with stable operation for over 2400 h under gradient current test conditions. Such precise molecular design and synthetic control provide valuable insights into structure-property relationships in advancing AEM materials, offering a promising pathway for enhancing the efficiency and durability of AEMWE systems.

2.1.4 | Solid Oxide Electrolysis

Solid oxide electrolysis cells (SOECs) operate at high temperatures, typically ranging from 500 to 1000°C, and can achieve an efficiency of up to 100% [51]. In an SOEC, water molecules at the cathode accept electrons and are reduced to form hydrogen gas and oxygen ions (O^{2-}), with hydrogen being released from the cathode surface. The oxygen ions migrate through the ion-conducting membrane to the anode, where they are oxidized to produce oxygen gas and electrons. Oxygen is released from the anode surface, while the electrons travel through an external circuit back to the cathode. A typical SOEC structure is shown in Figure 6. The anodic, cathodic, and overall reactions in solid oxide electrolysis are presented below [52]:

$$\text{Cathode reaction}: \quad H_2O + 2e^- \rightarrow H_2 + O^{2-} \quad (8)$$

$$\text{Anode reaction}: \quad 2O^{2-} \rightarrow O_2 + 2e^- \quad (9)$$

$$\text{Overall reaction}: \quad H_2O \rightarrow H_2 + \frac{1}{2}O_2 \quad (10)$$

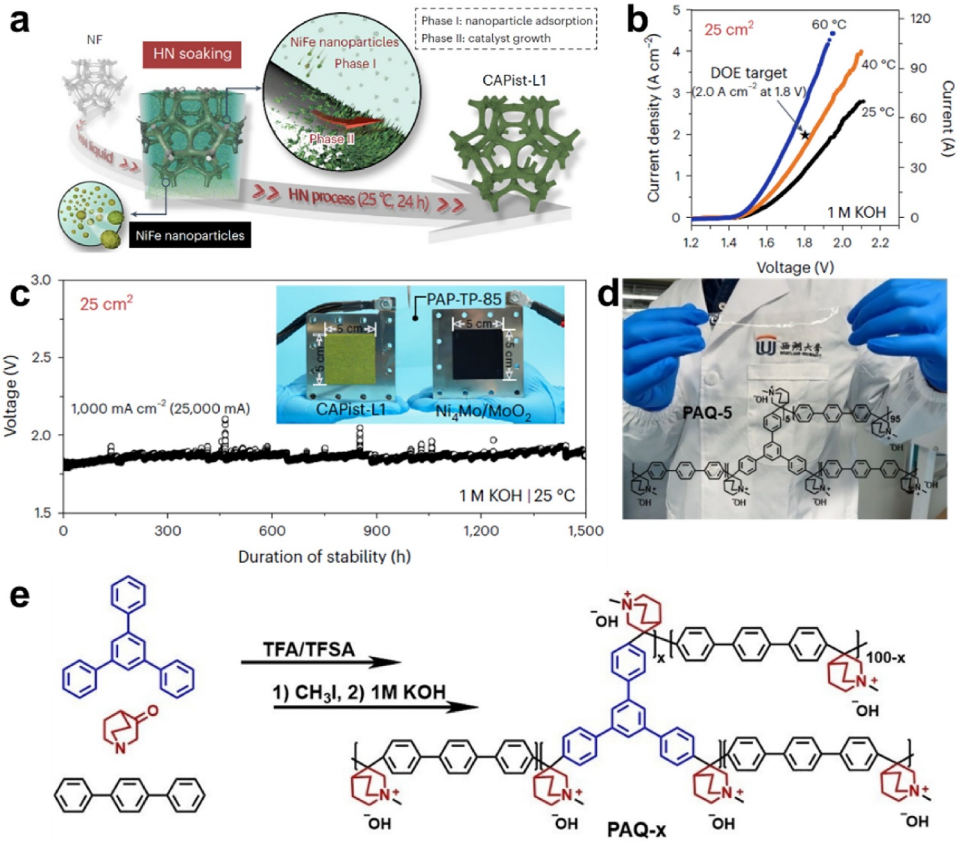

FIGURE 5 | (a) Schematic illustration of the preparation process for the CAPist-L1 catalyst via a one-step HN process, (b) Polarization curves of the 25 cm^2 electrolyzer at different operating temperatures, (c) Stability test of the 25 cm^2 electrolyzer at a current density of 1000 mA cm^{-2} and 25°C. Inset: Internal structure of the 25 cm^2 electrolyzer prior to testing, Reproduced with permission [49], Copyright 2024, Springer Nature. (d) Molecular structure and photographic image of PAQ-5, (e) Synthetic pathway of PAQ-x polymers, where x represents the molar ratio of 1,3,5-triphenylbenzene (TPB) in the copolymer, Reproduced with permission [50], Copyright 2024, Wiley.

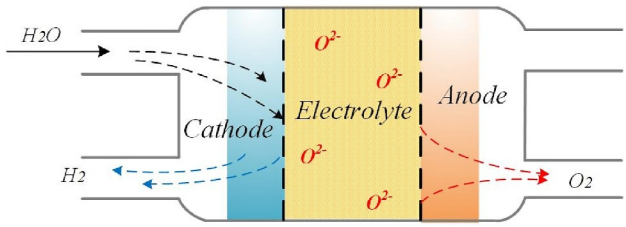

FIGURE 6 | The schematic diagram of SOEC.

The core components of a solid oxide electrolysis cell (SOEC) include the electrolyte, oxygen electrode, and fuel electrode. Currently, the most commonly used materials in SOECs include yttria-stabilized zirconia (YSZ) as the electrolyte, perovskite-based oxygen electrodes such as lanthanum strontium cobalt ferrite ($La_{1-x}Sr_xCo_{1-\gamma}Fe_\gamma O_{3-\delta}$, LSCF), and fuel electrodes composed of nickel-YSZ (Ni-YSZ) or nickel-gadolinium-doped ceria (Ni-GDC). These materials are chosen for their high ionic and electronic conductivity, thermal stability, and compatibility with high-temperature electrolysis conditions, ensuring efficient hydrogen production and long-term operational durability [53]. Salzgitter AG and Sunfire have successfully launched an industrial-scale SOEC project, producing 200 $Nm^3\ h^{-1}$ of green hydrogen at 850°C. The system operates with a nominal power input of 720 kW and achieves an impressive 84% electrical efficiency [54]. Meanwhile, in 2024, Mitsubishi Heavy Industries (MHI) initiated a 400-kW SOEC test module. This setup integrates multiple cartridges, each containing 500-cell stacks, and delivers an electrolytic efficiency of 3.5 kWh Nm^{-3} of hydrogen. At present, the deployment of SOECs is still at small scales due to their overall high costs, which also vary considerably among different manufacturers [55].

For solid oxide fuel cells (SOFCs), long-term operational stability is a critical factor for commercialization. It is reported that for SOEC stacks to achieve commercial viability, the degradation rate should be limited to approximately 1% per 1000 h or less [56]. Figure 7a compares the long-term stability of different SOEC systems [9]. Currently, some SOECs have demonstrated the potential to meet the durability requirements for commercial operation. Notably, the SOEC developed by Schefold et al. has achieved operational durations of up to 34,000 h at a current density of 0.6 A cm^{-2}, with a voltage degradation rate of 4–5 mV per 1000 h [60]. However, these tests have primarily been conducted at the laboratory scale. A major challenge for the large-scale deployment of SOEC technology lies in scalability. Future advancements will need to focus on increasing the surface area of individual cells beyond current limitations while integrating them into multi-cell stacks to enhance overall system efficiency and viability [61]. Figure 7b presents predictions for the capital cost of SOECs [9]. Currently, solid oxide electrolysis cells remain

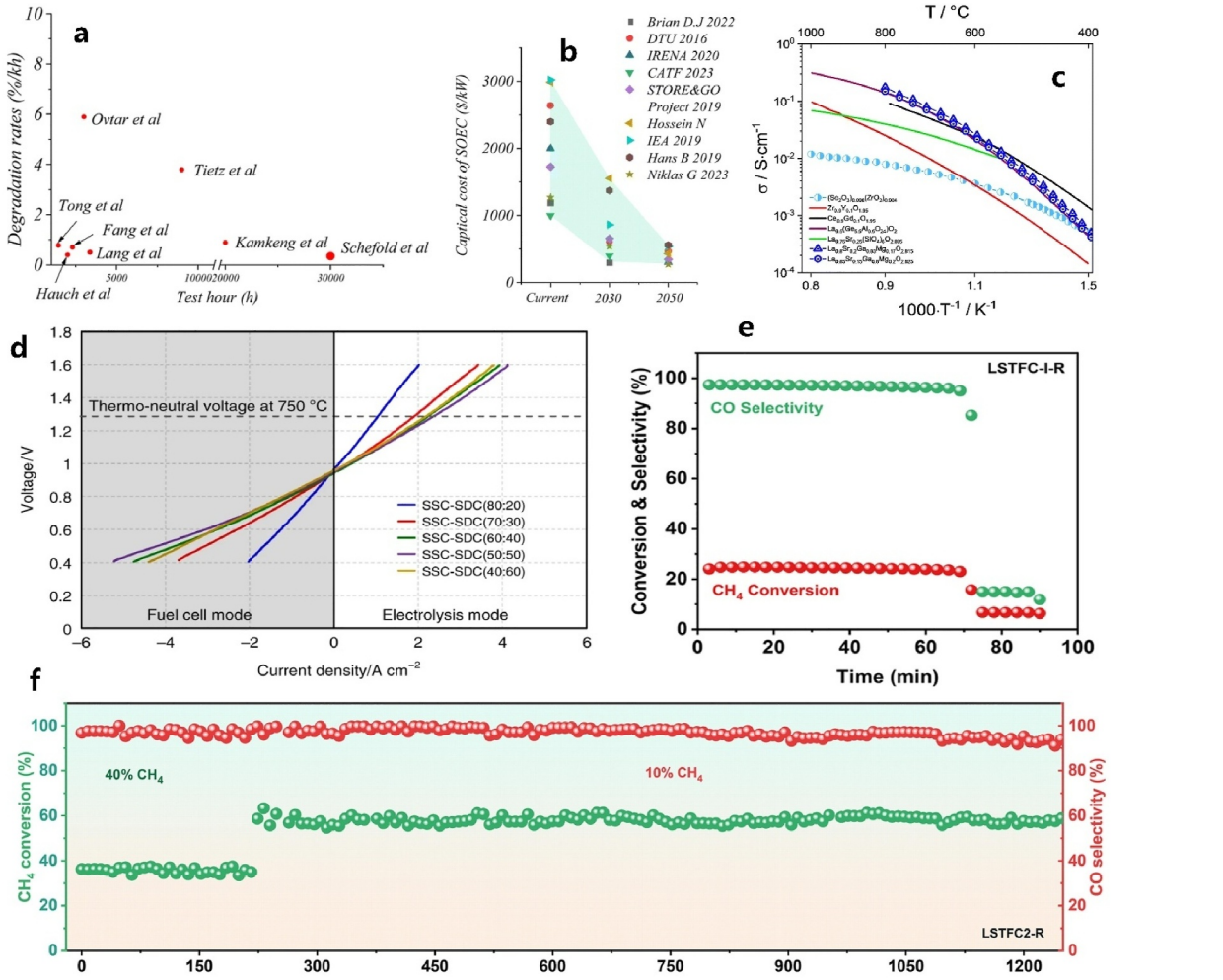

FIGURE 7 | (a) Long-term stability of different SOEC. (b) Predictions for the capital cost of SOECs, Reproduced with permission [9], Copyright 2024, Royal Society of Chemistry. (c) Total conductivity of commonly used oxide materials in SOECs, Reproduced with permission [57], Copyright 2023, Royal Society of Chemistry. (d) I-V characteristics in electrolysis and fuel cell modes with nanocomposite electrodes (SSC-SDC) at 750°C, Reproduced with permission [58], Copyright 2019, Springer Nature. (e) Stability test of LSTFC-I-R for anodic POM reaction. (f) Stability test of LSTFC2-R for anodic POM reaction, Reproduced with permission [59], Copyright 2024, Elsevier.

expensive, with prices varying significantly among manufacturers, ranging from 1000 to 3000 \$ kW^{-1}. The high costs are primarily due to limited large-scale production and application. However, with technological advancements and further scaling up, future costs are expected to decrease substantially, potentially reaching just 30% of current levels.

8YSZ is the preferred electrolyte material for SOECs due to its cost-effectiveness compared to alternatives such as scandia-stabilized zirconia (ScSZ) and gadolinium-doped ceria (GDC). Figure 7c illustrates the total conductivity of commonly used oxide materials in SOECs. Among them, doped ceria, a fluorite-type oxide, exhibits significantly higher ionic conductivity than stabilized zirconia in the intermediate temperature range of 600°C–800°C, making it a promising candidate for improving SOEC performance under moderate operating conditions [57]. Shimada et al. improved the performance of oxygen electrodes by optimizing both the chemical composition and the microstructure of the electrode materials. In this structure, nanoscale $Sm_{0.5}S_{0.5}CoO_{3-\delta}$ (SSC) and $Ce_{0.8}Sm_{0.2}O_{1.9}$ (SDC) particles are uniformly distributed, while submicron-sized particles interconnect to form continuous conductive pathways accompanied by wide pore channels, facilitating efficient gas diffusion and electron transport. Their system achieved current densities of 3.13 A cm^{-2} at 750°C and 4.08 A cm^{-2} at 800°C, corresponding to hydrogen production rates of 1.31 and 1.71 L h^{-1} cm^{-2}, respectively, which exceeds that of state-of-the-art electrolyzers [58]. To enable the large-scale application of SOECs in the future, it is essential to develop more advanced and stable materials that can enhance the activity of the electrolyzer and significantly extend its operational lifespan. Moreover, Figure 7d shows the I-V characteristics in electrolysis and fuel cell modes at 750°C, which indicates that the developed nanocomposite electrodes have great promise for applications in both SOFCs and reversible SOEC-SOFC systems [58]. Guo et al. employed an in situ exsolution strategy to generate stable CoFe alloy nanoparticles on the surface of a $La_{0.6}Sr_{0.4}Ti_{0.3}Fe_{0.5}Co_{0.2}O_{3-\delta}$ (LSTFC2) anode [59], leading to the development of a high-performance SOEC anode. During hydrogen production via the methane dry reforming reaction, the system achieved a CH_4 conversion rate of 86.9% and a CO selectivity of 90.1% (Figure 7e). It has demonstrated stable operation at 800°C for more than 1250 h with CO selectivity exceeding 95%

(Figure 7f), highlighting its great potential for efficient and long-lasting SOEC operation under hydrocarbon-rich conditions.

2.2 | Green Hydrogen Production From Water Splitting by Photocatalysis

Despite the significant advances of water electrolysis toward hydrogen, it remains a grand challenge for commercial success at a grid scale because of the high cost of the electrolyzers, the use of corrosive electrolytes, and extensive consumption of electricity. In contrast, photocatalytic water splitting provides an ideal alternative for the sustainable production of hydrogen with the only inputs of sunlight and water, showing remarkable advantages of the simplicity of the setup and low operational cost. This process mimics natural photosynthesis, utilizing semiconductor materials to directly convert sunlight into chemical energy in the form of hydrogen (Figure 8). Over the past few decades, significant progress has been made in this field. This section provides a brief review of the principles, materials, and advancements in photocatalytic water splitting, along with the challenges and prospects for scaling up this technology.

2.2.1 | Principles of Photocatalytic Water Splitting

Photocatalytic water splitting utilizes a photocatalyst under light irradiation to dissociate water (H_2O) into hydrogen (H_2) and oxygen (O_2). This process involves three fundamental steps (Figure 9 [62]):

The semiconductor photocatalyst absorbs photons with energy equal to or greater than its bandgap. This excites electrons from the valence band (VB) to the conduction band (CB), leaving behind holes in the VB. To achieve high solar-to-hydrogen conversion efficiency, maximizing light absorption is crucial, but this should not significantly compromise the semiconductor's redox potential. In principle, the semiconductor's energy bandgap must be greater than 1.23 eV. Moreover, the positions of the CB and VB must straddle the redox potential of overall water splitting. This alignment provides sufficient driving force for the reaction.

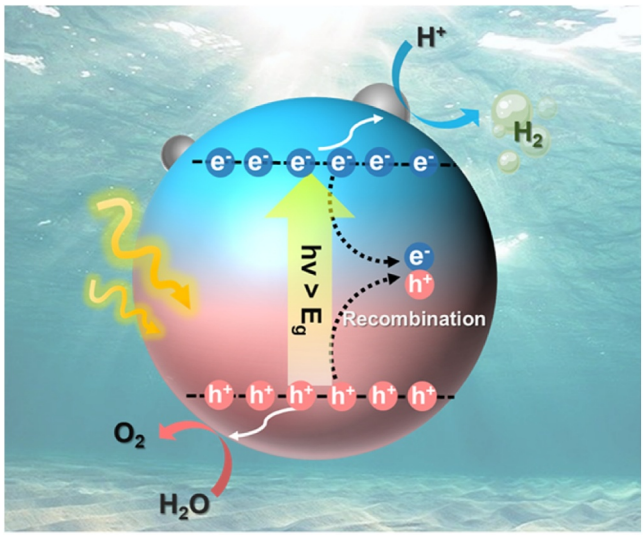

FIGURE 8 | The schematic illustration of solar-driven water splitting by photocatalysis.

The photoexcited electrons and holes then migrate toward the photocatalyst surface. Efficient charge separation is essential for high photocatalytic activity. However, a significant proportion of these charge carriers undergo severe recombination (both radiative and nonradiative), which remains a major bottleneck for efficient solar hydrogen production via overall water splitting.

In this final step, electrons drive the hydrogen evolution reaction while holes drive the OER on the photocatalyst surface. Although the thermodynamic minimum bandgap for water splitting is 1.23 eV, practical photocatalysts require a larger bandgap to overcome kinetic overpotentials and barriers. From a kinetic perspective, the OER, which involves a complex four-electron transfer, typically exhibits significantly slower reaction kinetics and higher activation barriers compared to the HER. To mitigate these overpotentials and enhance reaction kinetics, cocatalysts are broadly employed. These include: noble metals (e.g., Pt for HER; RuO_x, IrO_x for OER) and transition metal-based compounds (e.g., CoP, MoS_2 for HER; NiO_x for OER). However, photocorrosion remains a significant challenge for long-term stability, necessitating protective strategies (e.g., coatings, passivation layers) or the development of intrinsically stable photocatalytic materials.

2.2.2 | Recent Advances in Photocatalytic Water Splitting

In 1972, Honda and Fujishima reported groundbreaking research on photoelectrochemical water splitting in Nature [63]. For the first time, they constructed a bias-free system using a TiO_2 single-crystal photoanode and a Pt cathode, achieving overall water splitting ($2H_2O \rightarrow 2H_2 + O_2$) under ultraviolet light. This established the core mechanism of the "Honda-Fujishima Effect". This discovery not only demonstrated the feasibility of semiconductor-driven photolytic water splitting, but also, for the first time, established the critical design principle that the band positions of the catalyst must straddle the thermodynamic potentials of water splitting. However, the wide bandgap of TiO_2 (~3.0 eV) restricted its response to less than 5% of the solar spectrum, with a quantum efficiency below 1%, highlighting inherent bottlenecks in spectral absorption and charge separation efficiency. Benefitting from consideration efforts over the past decades, in 2021, Nishiyama and coworkers reported the world's first hundred-square-meter-scale photocatalytic hydrogen production system (Figure 10) [64]. Employing aluminum-doped strontium titanate ($SrTiO_3$: Al) catalyst sheets and an ultrathin reaction chamber design (0.1 mm gap), the system achieved a solar-to-hydrogen conversion efficiency of 0.76% under natural sunlight. An array of thousands of reaction units operated stably for several months, with a maximum daily hydrogen production reaching 19.9 mol. This validated the potential for large-scale application of photocatalytic technology.

In 2011, Wang et al. achieved photocatalytic overall water splitting using wafer-scale GaN nanowire arrays on silicon substrates, combined with a Rh/Cr_2O_3 core-shell co-catalyst

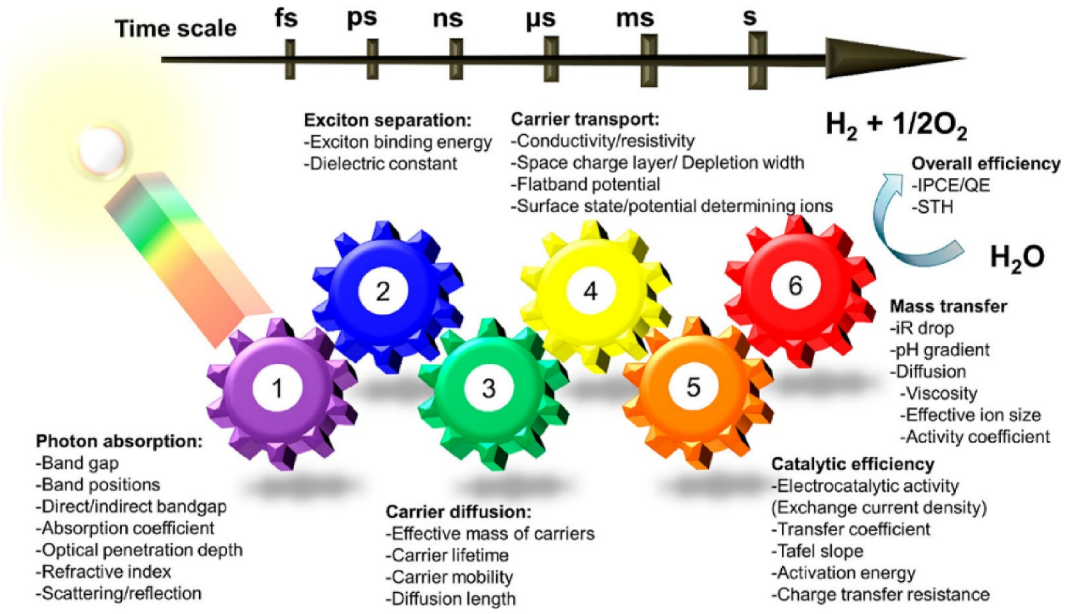

FIGURE 9 | Schematic illustration of three key steps of photocatalytic water splitting. Overall water splitting is only successful for high efficiencies of all six gears depicted in the scheme. The different time scales of the reactions are also displayed. Reproduced with permission [62], Copyright 2017, ACS Publications.

FIGURE 10 | An overhead view of the 100 m^2 solar hydrogen production system. Reproduced with permission [64], Copyright 2021, Springer Nature.

(Figure 11a) [65]. The vertically aligned nanowires (diameter ~50 nm) provided high-density nonpolar reaction interfaces, exhibiting a threefold enhancement in carrier migration efficiency compared to conventional powders. Figure 11b illustrates the typical temporal evolution of the photocatalytic water-splitting reaction under 300 W Xe lamp irradiation. Over the two cycles shown (~18 h), H_2 and O_2 were produced steadily and nearly stoichiometrically, with no observable decline in photocatalytic activity. Repeated experiments gave similar results. In 2023, Zhou et al. achieved a breakthrough in photocatalytic hydrogen production from water splitting via an infrared light-thermal synergy strategy using developed InGaN/GaN nanowires (Figure 11c), achieving a record-high solar-to-hydrogen (STH) efficiency of 9.2% under high-intensity simulated light (3800 $mW{\cdot}cm^{-2}$) (Figure 11d) [66]. The core breakthrough lay in utilizing infrared light (constituting 50% of the solar spectrum) to construct a self-heating system, precisely maintaining the reaction temperature at 70°C. Under these conditions, the hydrogen-oxygen recombination rate was significantly suppressed, while water dissociation kinetics were enhanced. More importantly, the technology demonstrated exceptional engineering compatibility: a large-scale 4 × 4 cm^2 reaction system still achieved a 6.2% STH efficiency under natural sunlight. Furthermore, it could directly decompose tap water and seawater, achieving stable hydrogen production efficiencies of 7.44% and 6.6%, respectively. This successfully eliminated the dependence of traditional photoelectrochemical hydrogen production on pure water and corrosive electrolytes.

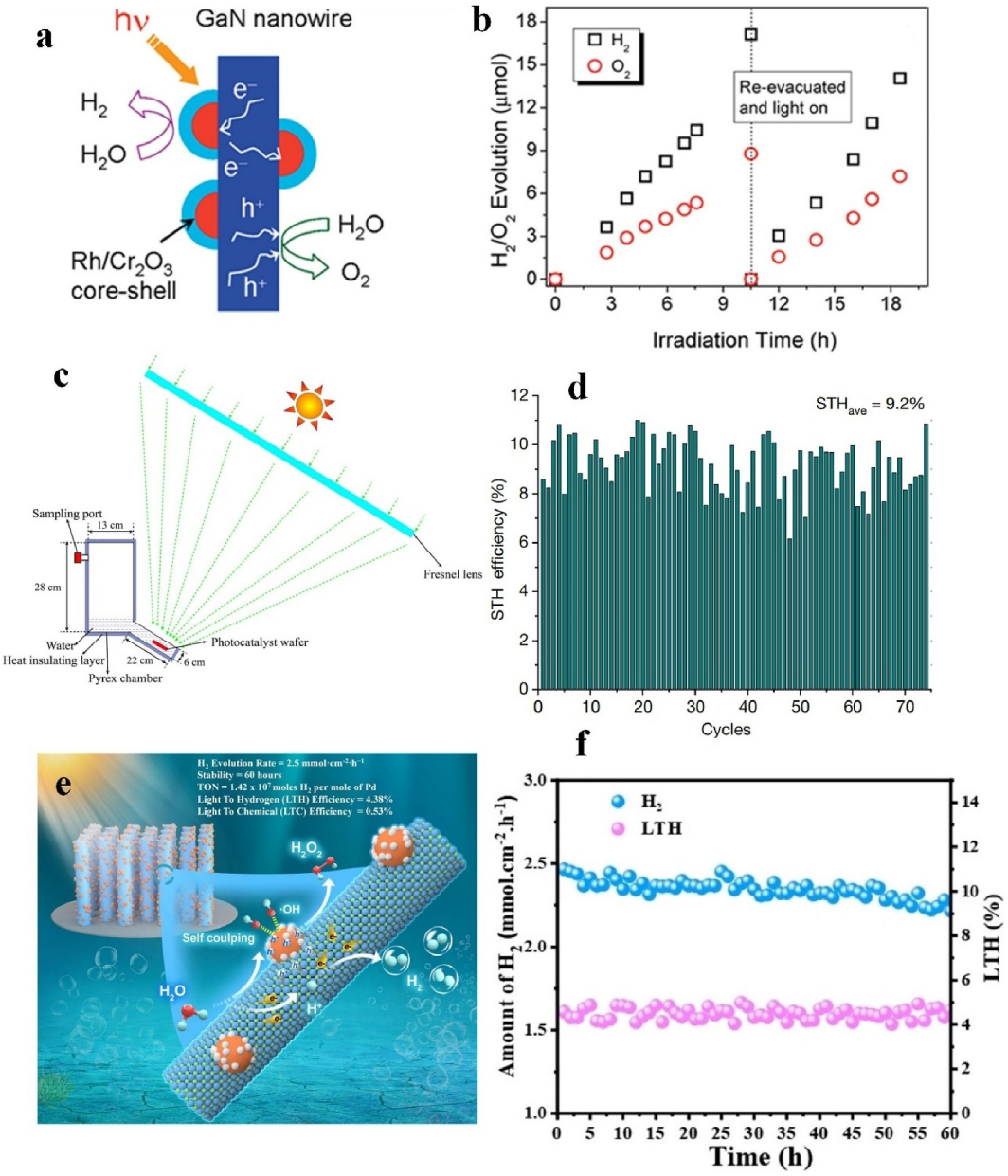

FIGURE 11 | (a) Schematic illustration of water splitting on GaN nanowires incorporating Rh/Cr_2O_3 core-shell nanostructures as cocatalysts. (b) Experimental overall photocatalytic water splitting was performed on GaN nanowires decorated with Rh/Cr_2O_3 core-shell nanostructures under 300 W full-arc xenon lamp irradiation for 18 h. Reproduced with permission [65], Copyright 2011, ACS Publications. (c) Schematic parameter illustration of the outdoor photocatalytic OWS system. (d) Stability test of $Rh/Cr_2O_3/Co_3O_4$-loaded InGaN/GaN nanowires in a self-heated photocatalytic overall water splitting system under concentrated light irradiation (3800 mW cm^{-2}). Reproduced with permission [66], Copyright 2023, Springer Nature. (e) Reaction mechanism of GaN nanowires decorated with Pd nanocluster for simultaneous production of H_2 and H_2O_2 from water splitting by photocatalysis. (f) Activity of H_2 production along with light-to-hydrogen (LTH) efficiency up to 60 h. Reproduced with permission [67], Copyright 2025, Wiley.

The novel paradigm of "light-thermal synergistic reaction modulation" established by this work paves the way for scaling up unassisted, zero-carbon-emission, solar-light-driven hydrogen production technology. In 2025, Nasir et al. developed an integrated Pd/GaN nanowires photocatalyst, pioneering a new pathway for the simultaneous production of hydrogen and hydrogen peroxide (H_2O_2) from seawater (Figure 11e) [67]. Under 3 W cm^{-2} light illumination, the system achieved a hydrogen production rate of 2.5 mmol cm^{-2} h^{-1} (photonic-to-hydrogen efficiency: 4.38%) and H_2O_2 generation of 300 μmol L^{-1}, operating stably for 60 h (Figure 11f). Mechanistic studies revealed that Pd nanoparticles functioned dually in hole extraction and intermediate regulation.

ABO_3-type perovskites (e.g., $SrTiO_3$, $LaCoO_{33}$) exhibit significant potential for photocatalytic water splitting due to their tunable bandgaps and high charge mobility. Recent advances highlight their promise for solar-driven hydrogen production from water splitting. Yu et al. [68] employed a fluoride-assisted nitridation strategy to engineer layered perovskite Sr_2TiO_4

(Figure 12a). By enhancing nitrogen doping and reducing defects, they achieved visible-light-driven overall water splitting with an apparent quantum efficiency (AQE) of 0.39% at 420 ± 20 nm and a solar-to-hydrogen (STH) efficiency of 0.028% (Figure 12b). Separately, Xiao et al. [69] synthesized sub-50 nm perovskite-type tantalum oxynitride $ATaO_2N$ (A = Sr, Ca, Ba) single nanocrystals (Figure 12c). After modification with Ir-Pt alloy@Cr_2O_3 cocatalysts, these nanocrystals exhibited significantly improved H_2 evolution, achieving an STH efficiency of 0.15% in a Z-scheme water splitting system, and the apparent quantum yield (AQY) for H_2 evolution was measured to be 4.0% at approximately 420 nm (Figure 12d). These strategies represent important progress in developing efficient perovskite photocatalysts for practical solar energy conversion applications.

In recent years, covalent organic frameworks (COFs) and metal-organic frameworks (MOFs) have garnered significant attention as next-generation photocatalysts for overall water splitting (OWS), owing to their modular architectures, high surface areas, and tunable electronic properties. Their structural precision enables the integration of active sites and functional units at the molecular level, offering unparalleled opportunities for the rational design of efficient photocatalytic systems. In the case of COFs, Qu and co-workers [70] pioneered the first example of visible-light-driven gas-phase OWS using a β-ketoenamine-linked COF (Pt@Tp-TAPyT-COF) incorporating triazine–pyridine moieties (Figure 13a). This system not only demonstrated efficient H_2 and O_2 production (51.2 and 25.6 μmol g^{-1} h^{-1}, respectively, under 88% relative humidity), but also effectively suppressed the backward oxygen reduction reaction—a common challenge in traditional liquid-phase systems. Detailed mechanistic studies revealed that carbonyl-O and pyridine-N sites functioned as dual-active centers, facilitating both water adsorption and redox catalysis. Moreover, the vapor-phase configuration eliminated interfacial limitations associated with aqueous systems, enabling long-term operational stability over 45 h. To further address the intrinsic limitations of charge separation and exciton recombination in COFs, Shen et al. [71] introduced a ground-state charge transfer (GSCT) strategy by engineering a co-planar single-molecule junction (FOOCOF-PDI) through covalent integration of electron donor–acceptor motifs (Figure 13b). This architecture exhibited a dramatically enhanced built-in electric field and dipole moment, which collectively promoted exciton dissociation and charge carrier migration. As a result, the material achieved an exceptional hydrogen evolution rate of 265 mmol g^{-1} h^{-1} under visible-light irradiation. Spectroscopic investigations, including ESR, SKPM, and transient absorption spectroscopy, provided compelling evidence for the GSCT effect and its critical role in sustaining long-lived charge-separated states, positioning this approach as a powerful design principle for future COF-based photocatalysts. In addition, Sun et al. [72] developed a structurally asymmetric MOF (CFA-Zn) comprising electronically isolated Zn^{2+} nodes and crystallographically independent linkers

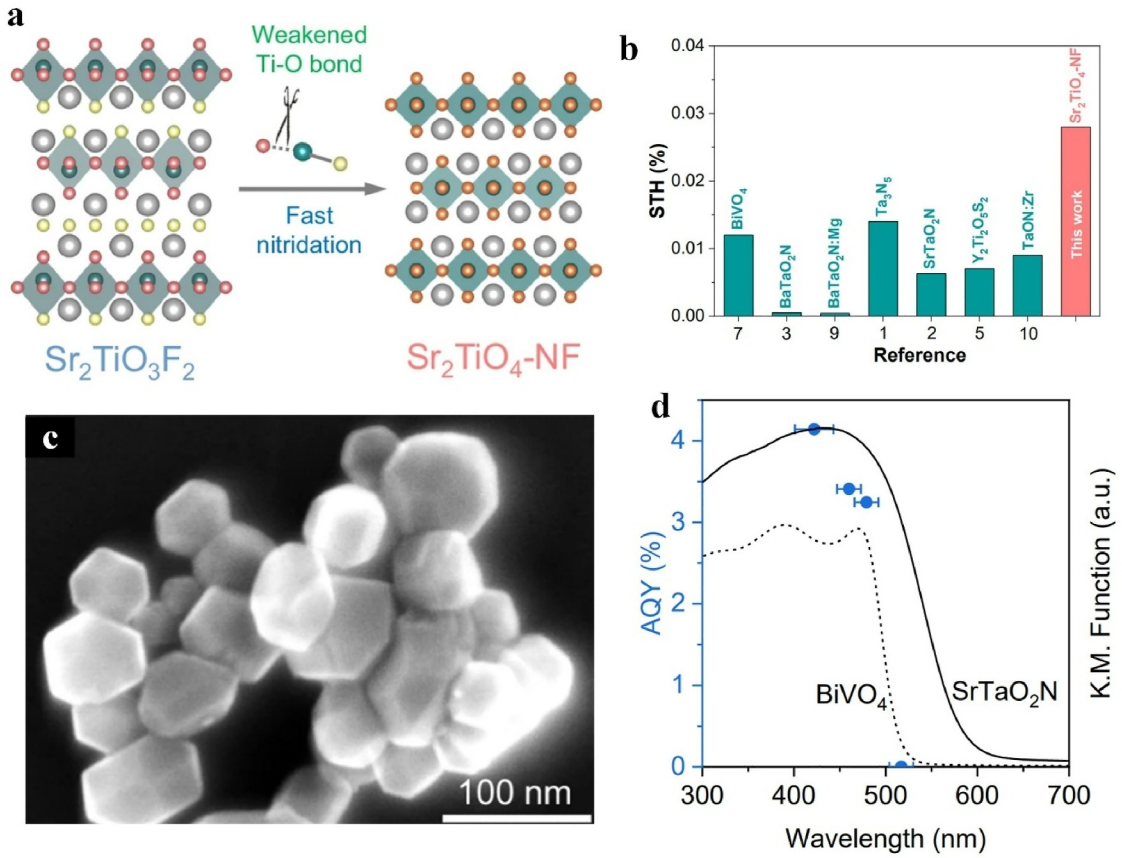

FIGURE 12 | (a) F-expedited nitridation of Sr_2TiO_4 using $Sr_2TiO_3F_2$. (b) Comparisons of visible-light-active compounds. Reproduced with permission [68], Copyright 2025, Springer Nature. (c) Scanning electron microscopy image of nanocrystalline $ATaO_2N$. (d) AQY as a function of the incident-light wavelength. Reproduced with permission [69], Copyright 2023, Springer Nature.

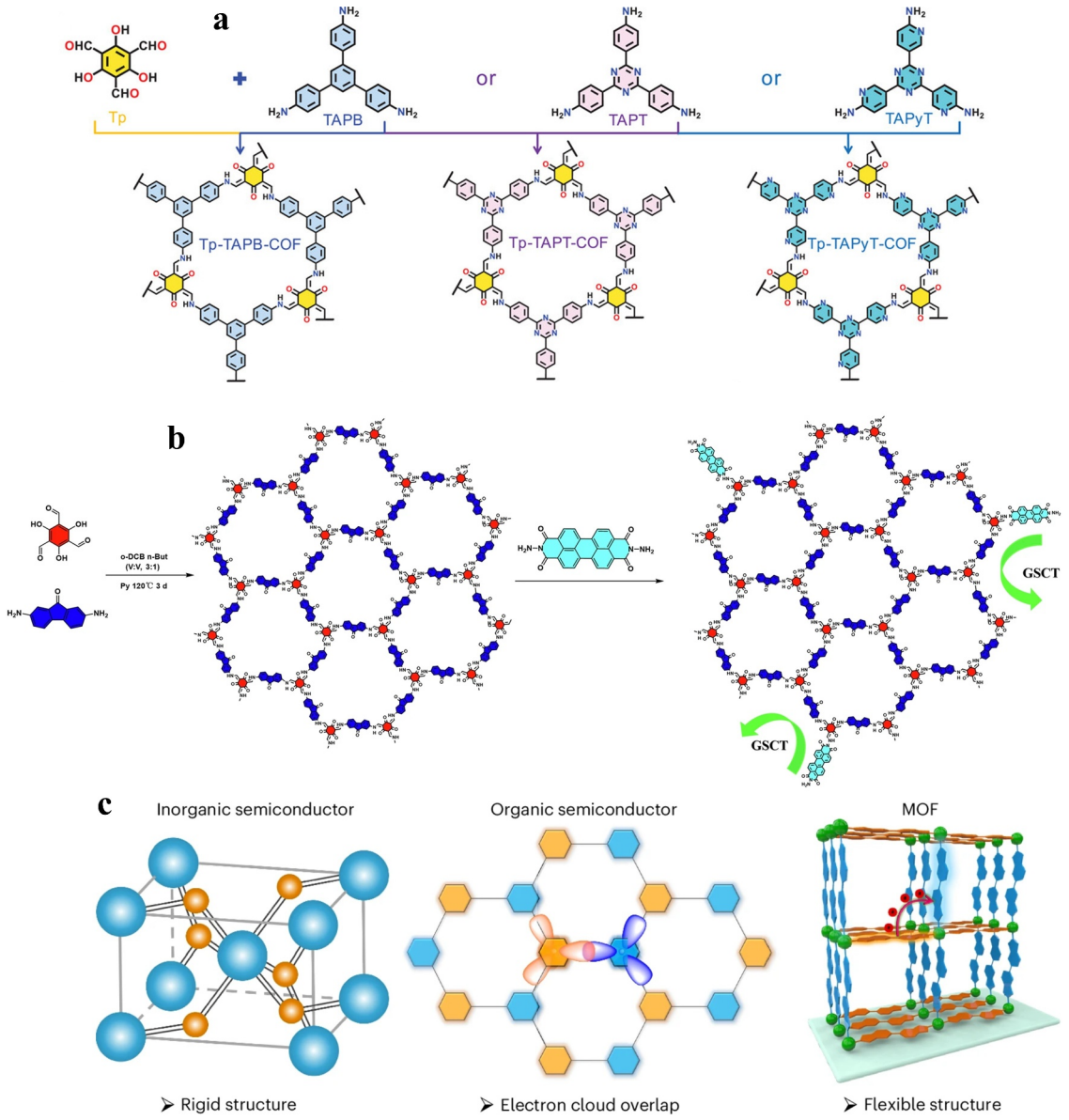

FIGURE 13 | (a) Synthetic scheme for the preparation and the structures of Tp-TAPyT-COF, Tp-TAPT-COF, and Tp-TAPB-COF. Reproduced with permission [70], Copyright 2025, Wiley. (b) Scheme of synthesis of the FOOCOF and FOOCOF-PDI. Reproduced with permission [71], Copyright 2025, Springer Nature. (c) Possible constructions of chemically segregated donor and acceptor systems for different types of photocatalysts. Reproduced with permission [72], Copyright 2024, Springer Nature.

functioning as a spatially segregated donor–acceptor pair. Upon visible-light excitation, the framework undergoes a dynamic excited-state structural twist, triggering orbital realignment and effectively forbidding radiative recombination pathways. This unique behavior resulted in a > 1000-fold increase in charge separation lifetime. Figure 13c gives the possible constructions of chemically segregated donor and acceptor systems for different types of photocatalysts [72]. With dual co-catalyst loading (Pt and Co_3O_4), the system achieved an apparent quantum efficiency of 3.09% at 365 nm and exhibited remarkable operational durability over 100 h. This biomimetic strategy, reminiscent of conformational gating in natural photosystems, underscores the importance of excited-state structural dynamics in suppressing recombination and enhancing OWS performance.

2.2.3 | Strategies to Achieve Practical Photocatalytic Water Splitting

Despite considerable efforts and significant advances, solar-driven water splitting by photocatalysis remains far from commercial viability due to persistent challenges: (i). Low Solar-to-Hydrogen Efficiency: Most photocatalysts exhibit STH efficiencies below 10% [73], primarily due to inefficient light absorption, severe charge recombination, and sluggish reaction kinetics. (ii). Limited Stability: State-of-the-art photocatalysts undergo rapid photo-corrosion and degradation under operational conditions in aqueous electrolytes [74]. (iii). Scalability Barriers: Translating laboratory-scale performance to industrially relevant systems while maintaining efficiency and cost-effectiveness presents critical hurdles [75].

Thus far, to address the aforementioned limitations of photocatalysts for efficient and stable hydrogen production via water splitting, several key strategies have been developed. (1) Narrowing bandgaps through metal/nonmetal doping or solid solution formation enables broadening light absorption (e.g., N-doped TiO_2) [76]. (2) Combining semiconductors with favorable band alignments (e.g., Type-II heterojunctions or Z-schemes) enhances charge separation and prolongs carrier lifetimes [77]. (3) Noble metals (e.g., Pt for HER) and transition metal compounds (e.g., Ni/Co-based) provide active sites and reduce reaction overpotentials [78]. (4) Nano-structuring (nanoparticles, nanowires, and nanosheets) increases surface area and shortens charge migration paths [79]. (5) Introducing oxygen vacancies or other defects improves light harvesting and charge separation efficiency [80].

To advance photocatalytic water splitting, future research should prioritize:

1. Novel Photocatalyst Development: Designing earth-abundant materials with optimal bandgaps, efficient charge separation, superior catalytic properties, and high stability is at the core of the achievement of solar hydrogen production [81, 82].
2. Advanced Characterization Techniques. Employing operando and time-resolved techniques to probe charge dynamics and atomic-scale reaction mechanisms. Key approaches include: Time-resolved spectroscopy (time-resolved photoluminescence—TRPL, transient absorption spectroscopy—TAS) tracking carrier lifetimes/separation kinetics [83]; Operando infrared spectroscopy (IR) detecting reaction intermediates (e.g., OH, OOH^-) and their transformations. Together, these complementary methods map carriers track—from generation and separation to migration to interface reactions, enabling rational design of photocatalysts for achieving breakthroughs in solar-to-hydrogen (STH) conversion efficiency, and ultimately promoting scalable and economically viable green hydrogen production.

By leveraging abundant resources like seawater and wastewater, coupled with concentrated solar energy, photocatalysis can transition from lab-scale curiosity to real-world application. The next decade will be pivotal in overcoming technical hurdles—such as improving catalyst durability and system scalability—to unlock the full potential of this technology. With continued innovation, photocatalysis may soon become a cornerstone of the global renewable energy infrastructure. Overall, photocatalytic water splitting holds immense potential for sustainable hydrogen production by directly leveraging abundant solar energy and water resources. While significant advancements have been made in understanding the fundamental principles and developing efficient photocatalysts, challenges related to efficiency, stability, and scalability must be addressed to realize their full potential. Continued interdisciplinary research, combining materials science, chemistry, and engineering, will be crucial for overcoming these barriers and paving the way for large-scale implementation of this technology.

3 | Novel Hydrogen Storage and Transportation Technologies

Figure 14a compares different hydrogen storage technologies in terms of their gravimetric and volumetric capacities [84, 85]. As shown, ammonia- and methanol-based hydrogen storage systems exhibit great potential due to their high gravimetric and volumetric hydrogen densities. However, the current cost of ammonia- and methanol-based technologies remains relatively high, and they are not well suited for small-scale applications. In addition, liquid organic hydrogen carriers (LOHCs) also possess relatively high hydrogen storage densities, but they face challenges such as difficult purification processes and poor cycle stability. Meanwhile, metal hydride-based hydrogen storage systems, owing to their flexible system configurations and operational safety, are more suitable for distributed or on-site hydrogen storage scenarios, such as renewable energy integration, backup power systems, or mobile hydrogen supply units. Figure 14b compares various adsorption-based hydrogen storage

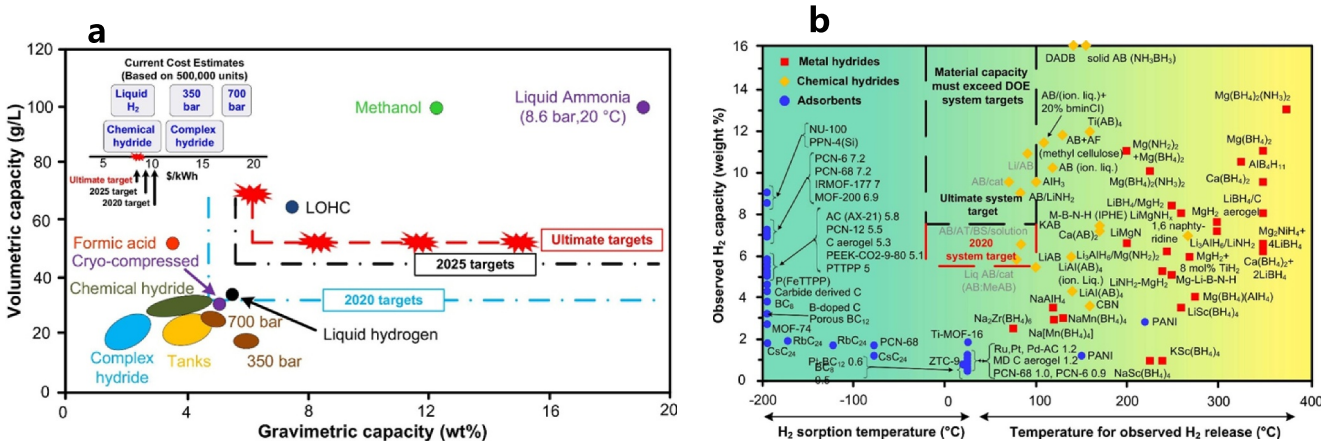

FIGURE 14 | Comparison of various hydrogen storage technologies. (a) Gravimetric and volumetric hydrogen densities for various storage technologies [84, 85]. (b) Hydrogen gravimetric capacity for H_2 storage materials based on adsorption-desorption temperatures (U.S. Department of Energy, Materials-Based Hydrogen Storage [86, 87]).

technologies, including metal hydrides [85–87]. As shown, different hydrogen storage materials exhibit distinct performance characteristics. High-temperature metal hydrides, represented by magnesium, possess relatively high hydrogen storage capacities—for example, magnesium offers a theoretical hydrogen capacity of approximately 7.6 wt.% [88], while $LiBH_4$ can achieve up to 18.4 wt.% [89]. In contrast, titanium-based metals can absorb and desorb hydrogen near room temperature but exhibit lower storage capacities. Moreover, metal-organic frameworks (MOFs) also demonstrate hydrogen adsorption capabilities; however, they typically require extremely low temperatures to achieve high performance—for instance, MOF-808 exhibits a volumetric hydrogen storage capacity of 50 g L^{-1} at 77 K and 100 bar [90].

The currently most mature technology is gaseous hydrogen storage, while liquid hydrogen storage involves high costs primarily due to its significant energy consumption and the construction of cryogenic storage tanks. For green ammonia and green methanol, the high costs mainly arise from the energy-intensive synthesis and hydrogen release processes. In addition, the cost of organic hydrogen storage carriers is also high, mainly because their catalysts contain precious metals. Similarly, magnesium-based solid-state hydrogen storage systems are cost-intensive mainly due to the high energy requirements during the hydrogen release process [7]. Because of differences in scale and technological maturity, the cost competitiveness of various hydrogen storage technologies is difficult to compare directly. Nevertheless, each technology has its own advantages and limitations, making it suitable for different application scenarios.

3.1 | Metal Hydrides-Based Hydrogen Storage and Transportation

Metal hydrides-based hydrogen storage technique relies on the reversible reaction between metals or alloys and hydrogen to form metal hydrides. As shown in Figure 15 [91], taking magnesium as an example, the hydrogenation process typically follows four key steps: physisorption of H_2 molecules on the surface, dissociation of H_2 into hydrogen atoms, chemisorption of atomic hydrogen, and finally, diffusion of hydrogen atoms into the bulk of the magnesium. This sequence represents the characteristic mechanism of hydrogen absorption in magnesium-based systems. Currently, the commonly used hydrogen storage materials include rare-earth alloys, titanium-based alloys, magnesium-based alloys, and vanadium-based alloys. These materials exhibit distinct hydrogen storage capacities and operate at different absorption/desorption temperatures. For example, titanium- and vanadium-based alloys typically react at lower temperatures but offer relatively limited hydrogen storage capacity. Rare-earth alloys, such as $LaNi_5$, provide good performance but are associated with high material costs. In contrast, magnesium-based alloys have the advantage of high hydrogen storage density (7.6 wt% for MgH_2), yet their hydrogen absorption and desorption occur at elevated temperatures (~300°C), resulting in the increased energy consumption during operation.

Currently, solid-state hydrogen storage materials have been successfully commercialized at various scales. For instance, Anqing Xuanda has launched a flexible production line with an annual capacity of 3000 tons, capable of manufacturing a range of hydrogen storage alloys, including rare-earth AB_5-type, Ti-Mn-based AB_2-type, Ti-Fe-based AB-type, and rare-earth Mg-Ni-based alloys [94]. Hydrexia (China) has developed a magnesium-based solid-state hydrogen storage and transportation vehicle equipped with a 20-foot hydrogen storage container. Each container can store up to 1 ton of hydrogen, achieving a material based hydrogen storage capacity of 6.4 wt% [95]. Although solid-state hydrogen storage has gained market attention due to its excellent safety advantages, its large-scale future deployment still depends on the development of advanced hydrogen storage materials and the integration of efficient storage systems.

From the materials perspective, current research primarily focuses on strategies such as adding catalysts and engineering

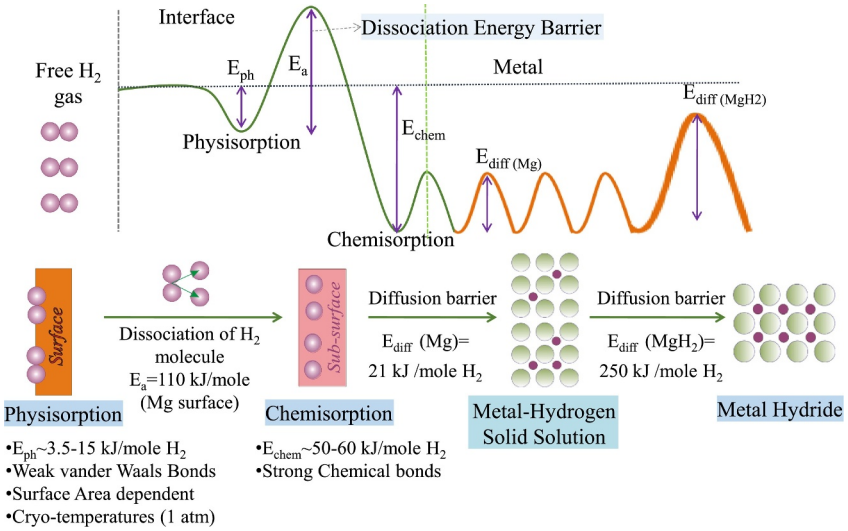

FIGURE 15 | Reaction mechanism of hydrogen and metals/alloys combination processes, Reproduced with permission [91], Copyright 2021, Elsevier.

nanostructured hydrogen storage materials. These approaches aim to enhance both the kinetic and thermodynamic properties of the materials, while also increasing hydrogen storage density. These approaches aim to enhance the kinetic and thermodynamic properties of the material while increasing the hydrogen storage density. Zhang et al. developed a single-phase Mg_2Ni (Cu) alloy through atomic reconstruction to achieve an optimal combination of photothermal and catalytic effects for stable, solar-driven hydrogen storage in MgH_2 [92]. This design enables the complete dehydrogenation of MgH_2 within 15 min under a solar irradiation intensity of 3.5 W cm^{-2}, delivering a reversible hydrogen storage capacity of ~6.1 wt%. As illustrated in Figure 16a, the repeated in situ atomic reconstruction during cycling facilitates the synergistic integration of photothermal conversion and catalytic activity, maintaining 95% of the storage capacity after 10 cycles powered solely by solar energy (Figure 16b). Huang et al. synthesized Ni/MnO nanocomposites directly from one-pot bimetallic MOFs, which were subsequently utilized as efficient catalysts to enhance the hydrogen storage performance of MgH_2. Among them, the MgH_2-10 wt.% Ni_1Mn_1-MOF-derived composite exhibited excellent overall performance, with a saturated hydrogen capacity of 6.42 wt%, and fast hydrogen release and uptake kinetics (Figure 16c) [93].

On the system level, current research focuses on the design of advanced hydrogen and thermal integrated systems/tanks, aiming to achieve flexible and efficient hydrogen storage and transportation. Optimizing the heat exchange structure of fins within hydrogen storage tanks is considered one of the most effective strategies to enhance hydrogen storage efficiency. Lesmana et al. combined the SIMP (Solid Isotropic Material with Penalization) filtering method with topology optimization to tailor the properties of metamaterials (Figure 17), thereby improving the volumetric efficiency of metal hydride (MH) reactors [96]. As a result, the reactor volume increased significantly by 66.22%, while both gravimetric and volumetric efficiencies were improved. Additionally, the hydrogen storage capacity was enhanced by 49%. Moreover, another promising approach involves integrating hydrogen storage systems with advanced thermal energy storage technologies, which can significantly enhance overall hydrogen storage efficiency. This integration allows for better thermal management during hydrogen absorption and desorption processes, ultimately improving system responsiveness and reducing energy losses. Current MH tanks face several challenges, including low energy efficiency, high levelized costs of hydrogen storage, slow hydrogen absorption and desorption rates, and complex thermal transfer structures inside the MH tanks that occupy a significant amount of space.

3.2 | Liquid Organic Hydrogen Carriers-Based Hydrogen Storage and Transportation

Liquid organic hydrogen carriers (LOHCs) represent a hydrogen storage method based on the reversible hydrogenation and dehydrogenation of organic liquid carriers, where the hydrogen storage process by LOHCs based on renewable energy is illustrated in Figure 18 [97]. An ideal LOHC should exhibit excellent thermal and chemical stability, be capable of long-term cycling, offer high hydrogen storage density, and ensure safety, high efficiency, and low cost. Currently, widely studied and utilized LOHC materials include benzene, toluene, naphthalene, N-ethylcarbazole, dibenzyltoluene, etc. Among these, Japan's Chiyoda Corporation has successfully commercialized the toluene/methylcyclohexane (TOL/MCH) system [98], while Germany's Hydrogenious Technologies has developed a hydrogen storage based on the dibenzyltoluene (DBT),

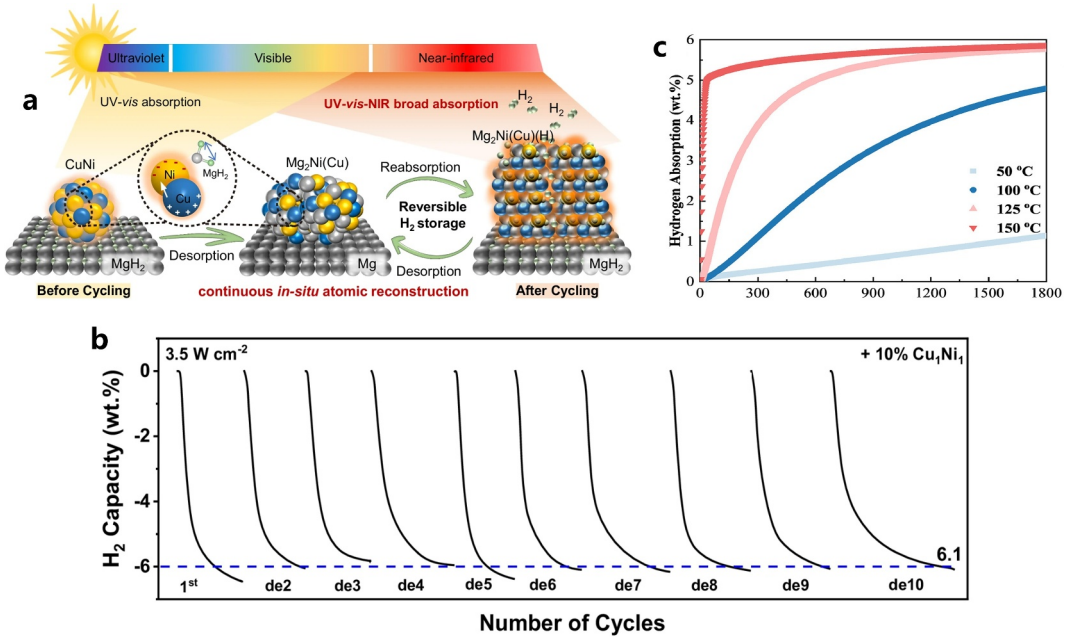

FIGURE 16 | (a) Schematic diagram of the ideal integration of photothermal and catalytic effects via continuous in situ atomic reconstruction upon repeated dehydrogenation process, Reproduced with permission [92], Copyright 2024, Springer Nature. (b) Cycling H_2 desorption curves of MgH_2 under the catalysis of Cu_1Ni_1 using a light intensity of 3.5 W cm^{-2}. (c) Isothermal absorption curves of MgH_2–10 wt.% Ni_1Mn_1–MOF derivative at different temperatures (50, 100, 125, and 150°C), Reproduced with permission [93], Copyright 2024, Elsevier.

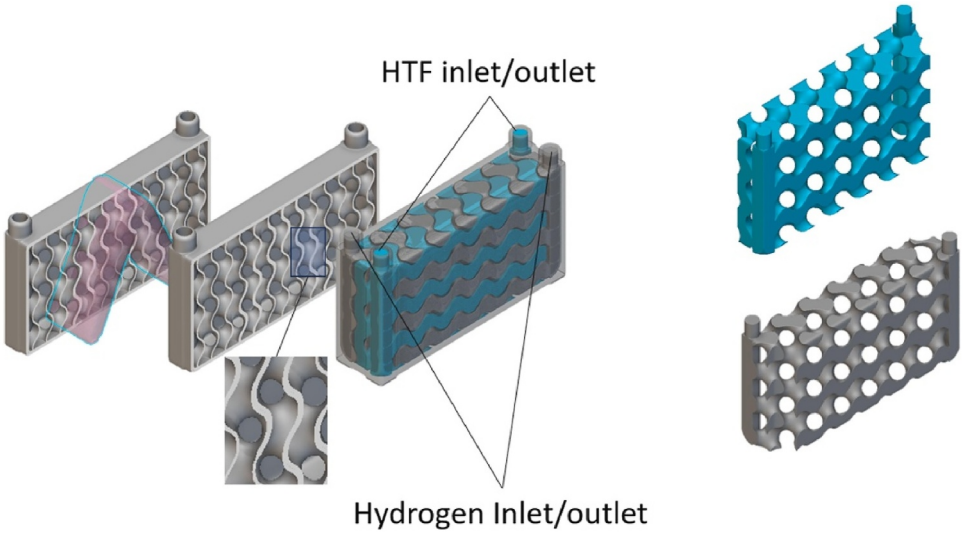

FIGURE 17 | Visualization of the final reactor model and thickness generated based on the TO mapping method, and two chambers extracted from the inner region of the reactor in the nonoffset configuration, Reproduced with permission [96], Copyright 2024, Elsevier.

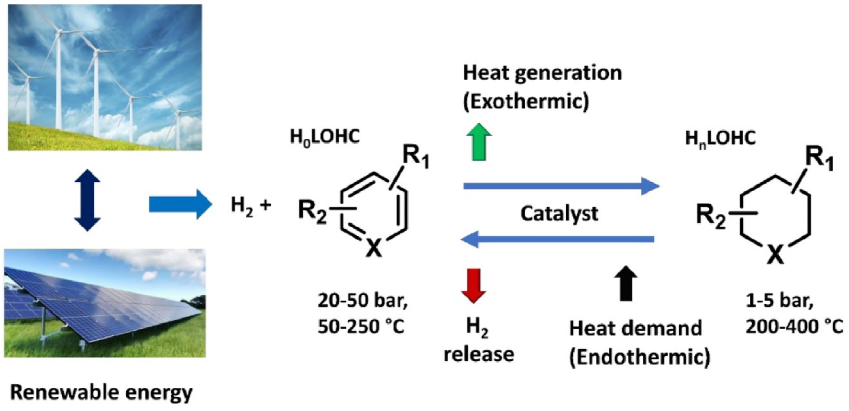

FIGURE 18 | Schematic diagram of the LOHC process, Reproduced with permission [97], Copyright 2020, MDPI.

which enables easy handling of hydrogen, offers excellent safety, and can be reused over a hundred cycles without significant degradation [99].

The development of efficient, stable, and low-cost catalysts is a critical factor for enabling the large-scale deployment of LOHC technology. The catalyst plays a crucial role in determining both the conversion rate and selectivity in hydrogenation of liquid organic carriers. The effectiveness of hydrogenation catalysts largely depends on the active components supported on the catalyst carrier. Common catalysts are generally classified into two categories: noble metals and non-noble metals [100]. Among them, noble metal catalysts—particularly ruthenium (Ru) and Pt—are highly valued for their excellent corrosion resistance, oxidation resistance, thermal stability, and superior catalytic activity [101]. The Ru nanocluster/Ni/NiO nanoparticle catalyst has been reported to demonstrate exceptionally high catalytic performance in the hydrogenation of benzene, up to 55 times greater than that of conventional Ru-Ni alloys or Ru catalysts supported on Ni. A distinctive feature of this catalyst lies in its structure: ultra-small, well-dispersed Ru nanoclusters are anchored onto the surface of Ni/NiO nanoparticles (Shown in Figure 19a). The activation of benzene primarily occurs at the NiO sites, where the π-electrons of benzene interact with the positively charged vacancies in the nickel oxide, facilitating adsorption and subsequent hydrogenation [102]. Figure 19b shows the dehydrogenation rate curves of 12H-N-ethylcarbazole (12H-NEC) over different catalysts at 179.85°C. Jiang et al. reported that Pt/TiO_2 exhibited superior catalytic performance and selectivity in the dehydrogenation of 12H-NEC compared to Pd/TiO_2 and commercial Pd/Al_2O_3. Among the noble metal catalysts tested, the catalytic activity followed the order: Pt/TiO_2 > Pd/TiO_2 > Rh/TiO_2 > Au/TiO_2 > Ru/TiO_2, indicating that Pt-based catalysts are the most effective under the given conditions [103]. Schörner et al. investigated the dehydrogenation of perhydro-dibenzyltoluene (H18-DBT) utilizing Pt-based catalysts designed for inductive heating. As shown in Figure 19c, the cross-sectional SEM image and elemental mapping of the Al_2O_3@Al_2O_3–IO–Pt composite reveal its structured morphology and uniform elemental distribution. Figure 19d compares hydrogen generation rates and recorded bulk temperatures against the degree of dehydrogenation (DoD), highlighting the differences in efficiency between conventional thermal heating and inductive heating approaches [104]. The results indicate that inductive heating is a highly promising technology that can minimize heat loss to

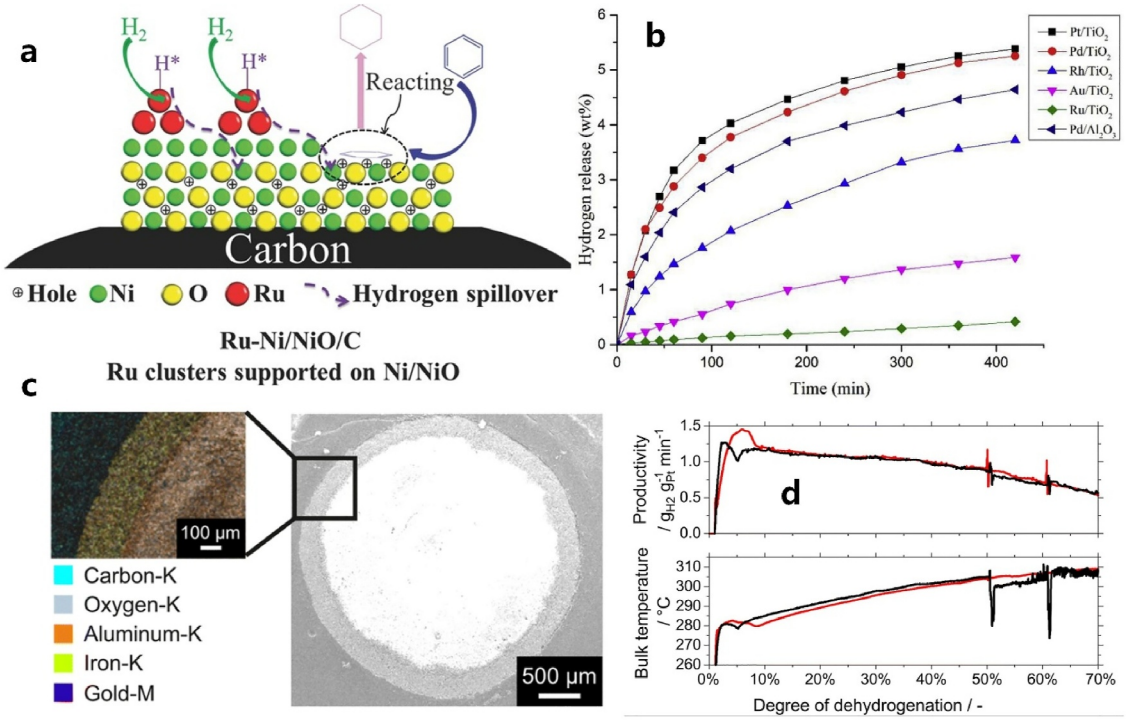

FIGURE 19 | (a) The hydrogenation mechanism of benzene over the Ru–Ni/NiO/C catalyst, Reproduced with permission [102], Copyright 2015, Wiley. (b) Hydrogen release curves from 12H-NEC dehydrogenation over various M/TiO_2 and Pd/Al_2O_3 catalysts at 453 K, Reproduced with permission [103], Copyright 2019, Elsevier. (c) Cross-sectional SEM image of the $Al_2O_3@Al_2O_3$–IO–Pt composite along with its corresponding elemental distribution map (d) The hydrogen generation rates and bulk temperatures against the degree of dehydrogenation using $Al_2O_3@Al_2O_3$–IO–Pt as the catalyst, Reproduced with permission [104], Copyright 2024, Royal Society of Chemistry.

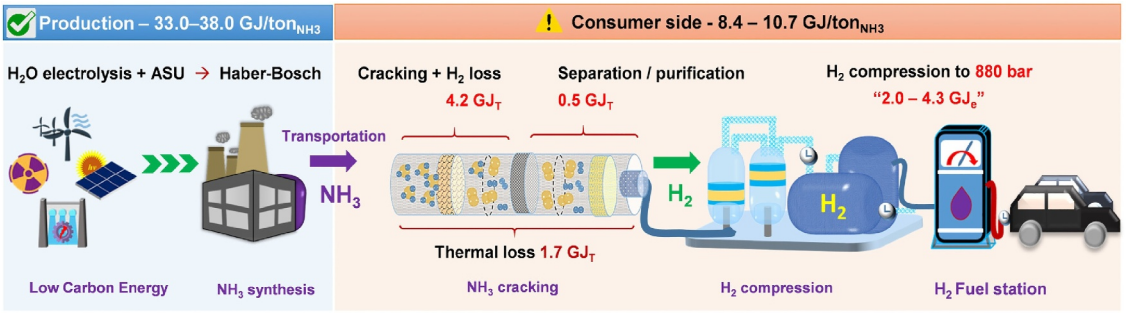

FIGURE 20 | Energy consumption in the power-to-power cycle when using ammonia as a hydrogen carrier, Reproduced with permission [106], Copyright 2021, American Chemical Society.

the environment and enhance the responsiveness of on-demand hydrogen release.

3.3 | Ammonia-Based Hydrogen Storage and Transportation

Ammonia is a carbon-free clean energy carrier, offering a high hydrogen content (17.65 wt%), excellent volumetric hydrogen density (107.7 g/L), and a high energy density (21.18 MJ/kg), along with the advantage of an already well-established infrastructure [105]. However, current challenges in ammonia-based hydrogen storage include the high cost of green ammonia production, significant energy requirements for ammonia cracking, as well as the corrosive and toxic nature of ammonia itself. Figure 20 illustrates a typical energy supply pathway for hydrogen storage and utilization via ammonia. The ammonia cracking process involves substantial energy losses, thermal losses of approximately 1.7 GJ per ton of NH_3, and additional electrical losses of 2.0–4.3 GJ per ton of NH_3 due to hydrogen compression [106]. As a result, the overall conversion efficiency at the point of use is limited to about 61.0%–68.5%.

Reducing energy consumption is a major focus in current research on ammonia-based hydrogen storage and transportation, especially in the processes of ammonia synthesis and decomposition. For example, Chang et al. developed a transition metal free catalyst, potassium hydride intercalated graphite ($KH_{0.19}C_{24}$), which can activate dinitrogen under relatively mild temperature and pressure conditions [107]. The catalyst's

performance varies with different potassium hydride loadings in the precursor (1–30 wt%). The catalyst prepared with 20 wt% KH loading exhibited the highest ammonia production rate at 250°C–400°C and 1 MPa, showing a performance comparable to that of the traditional noble metal catalyst Ru/MgO [107]. Tabassum et al. reported a novel ruthenium-free catalyst composed of CoNi alloy nanoparticles dispersed on a potassium-modified MgO-CeO_2-SrO mixed oxide support. This catalyst achieved an impressive ammonia conversion efficiency of up to 97.7% at 450°C and delivered a hydrogen production rate comparable to that of Ru-based catalysts at 500°C, while also demonstrating excellent long-term stability during continuous operation [108].

3.4 | Methanol-Based Hydrogen Storage and Transportation

Methanol-based hydrogen storage offers a combination of advantages, including high hydrogen content, ease of storage and transport in liquid form, mature infrastructure, renewable production pathways, mild dehydrogenation conditions, and strong compatibility with fuel cells. It has a gravimetric hydrogen density of 12.5 wt%, a volumetric hydrogen density of 99 g L^{-1} [109]. Typical methods for methanol synthesis include hydrogenation of syngas and hydrogenation of CO_2.

Figure 21 illustrates a typical process flow for methanol synthesis via CO_2 hydrogenation [110]. In this pathway, captured CO_2 is mixed with electrolytic hydrogen produced from water electrolysis in an intercooling compressor. The heated H_2/CO_2 feed gas is then pressurized to about 65 bar and fed into a reactor where methanol is directly synthesized via hydrogenation of CO_2. Currently, state-of-the-art technology typically employs reactors equipped with copper-based catalysts, such as $CuO/ZnO/Al_2O_3$ composites. Moreover, the catalyst's structure and composition significantly influence the reaction performance. Copper-based catalysts are widely favored in industry due to their excellent activity and selectivity. Reaction temperatures are typically controlled within the range of 200°C–300°C to balance reaction rate and catalyst stability [111]. This process not only effectively utilizes captured CO_2 to enable carbon recycling but also integrates green hydrogen produced via water electrolysis, offering notable environmental benefits and strong potential for sustainable development.

4 | Green Hydrogen Applications

Hydrogen serves as both an energy carrier and a chemical feedstock. As an energy carrier, the large-scale deployment of hydrogen can significantly increase the penetration of renewable energy into the power grid, playing a key role in enabling a sustainable energy supply system. In addition to electricity generation, hydrogen can be used as a fuel for residential and district heating, as well as for powering trains, aircraft, and ships. Owing to its strong reducing properties, hydrogen is also well-suited for applications in steel production and the synthesis of major chemical products such as ammonia, methanol, and olefins. Because of its broad applicability across sectors, the large-scale development of hydrogen is essential to achieving deep decarbonization. Figure 22 illustrates hydrogen's potential contribution to global CO_2 abatement by 2050 across various sectors [112]. From now until 2050, hydrogen has the potential to cumulatively reduce CO_2 emissions by 80 GT-equivalent to approximately 11% of the total reductions needed to limit global warming to 1.5°C–1.8°C.

4.1 | Hydrogen Power Generation

Hydrogen energy is primarily applied in the power generation sector through fuel cell technology. Because of its high efficiency and zero-emission electricity generation, fuel cell technology is currently regarded as a highly promising solution for power generation. Table 2 summarizes the features of different fuel cell technologies [113–116]. Among the various fuel cell technologies, proton exchange membrane fuel cells (PEMFCs) are currently the

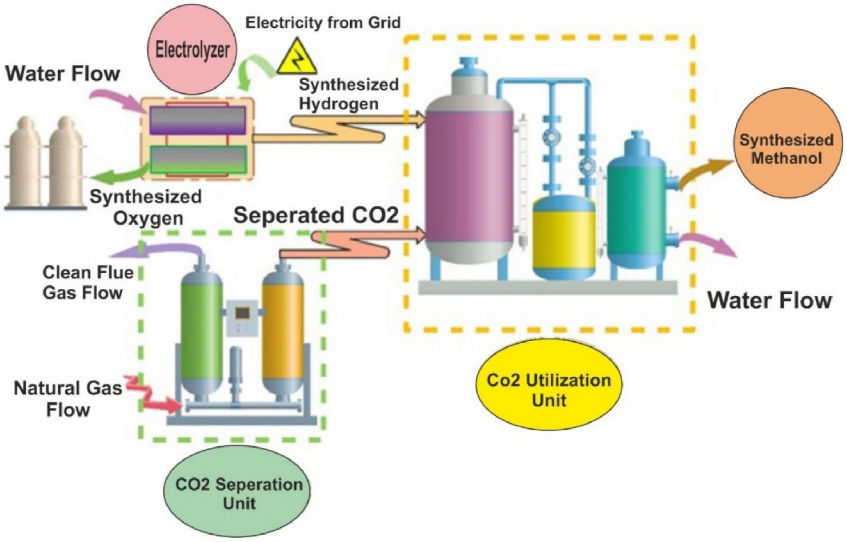

FIGURE 21 | Diagram of methanol synthesis from CO_2 hydrogenation, Reproduced with permission [110], Copyright 2022, Elsevier.

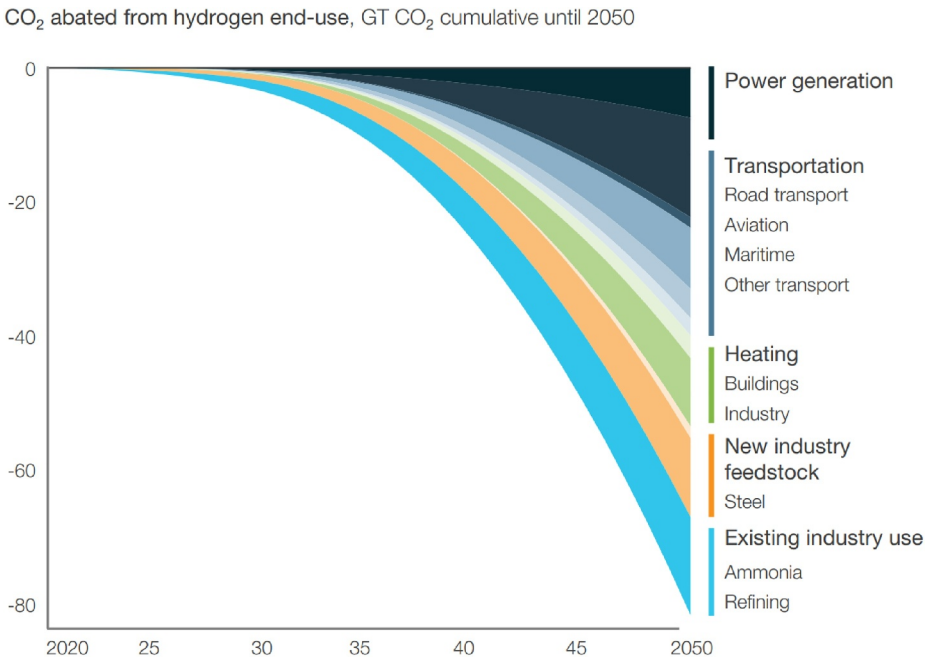

FIGURE 22 | Hydrogen's potential contribution to global CO_2 abatement by 2050 across various sectors (Hydrogen Council [112]).

TABLE 2 | Comparison features of different fuel cell technologies [113–116].

Item	PEMFC	PAFC	AFC	SOFC	MCFC
Operating temperature (°C)	< 120°C	150°C–200°C	< 100°C	600°C–1000°C	600°C–700°C
Cell voltage (V)	1.1	1.1	1	0.8–1.0	0.7–1
Power density (W/cm^2)	0.35–0.36	0.17–0.19	0.1–0.3	0.24–0.3	0.1–0.2
Electrical efficiency (%)	40%–60%	40%	60%	60%	50%
Advantages	Rapid start-up and load following; flexible adjustment; high power density	Low pollutions; suitable for CHP; maturity of technology	Low start-up temperature; high efficiency; quick start-up	High efficiency; fuel flexibility; waste heat utilization to further improve efficiency	Fuel flexibility; suitable for CHP
Challenges	Expensive catalysts; high purity hydrogen; sensitive to impurities	Expensive catalysts; less powerful; slow start-up	Sensitive to CO_2; corrosiveness	Slow start-up and load following; big thermal lag	Slow start-up; corrosiveness

most widely used due to their fast response speed, technological maturity, and high-power density. However, PEMFCs are still relatively expensive and highly sensitive to fuel impurities such as carbon monoxide and sulfur compounds, which can impair their performance and durability. In contrast, solid oxide fuel cells (SOFCs) have attracted increasing attention for their excellent fuel flexibility, high operating temperatures (600°C–1000°C), and high electrical efficiency, which can reach up to 60% and even higher when used in combined heat and power systems [117]. Despite these advantages, SOFCs face significant challenges, including slow start-up times and limited load-following capabilities, which complicate their control strategies. Besides, hydrogen-fueled gas turbines have the potential to achieve zero carbon emissions during combustion [18]. However, hydrogen has unique burning characteristics, such as higher flame speed, wider flammable range, and lower ignition energy. These features can affect the stability of combustion, the behavior of the flame, and the overall burning process in the turbine. Therefore, major modifications to the turbine and its combustion system are needed to ensure safe and reliable operation [118].

4.2 | Hydrogen-Powered Transportation

Hydrogen is a potential alternative fuel for the future transportation sector, capable of powering aircraft, ships, and vehicles. The transportation sector accounts for approximately 25% of global carbon emissions, highlighting the urgent need to identify alternative clean fuels [18]. In the maritime and aviation sectors, the focus is primarily on hydrogen combustion for propulsion,

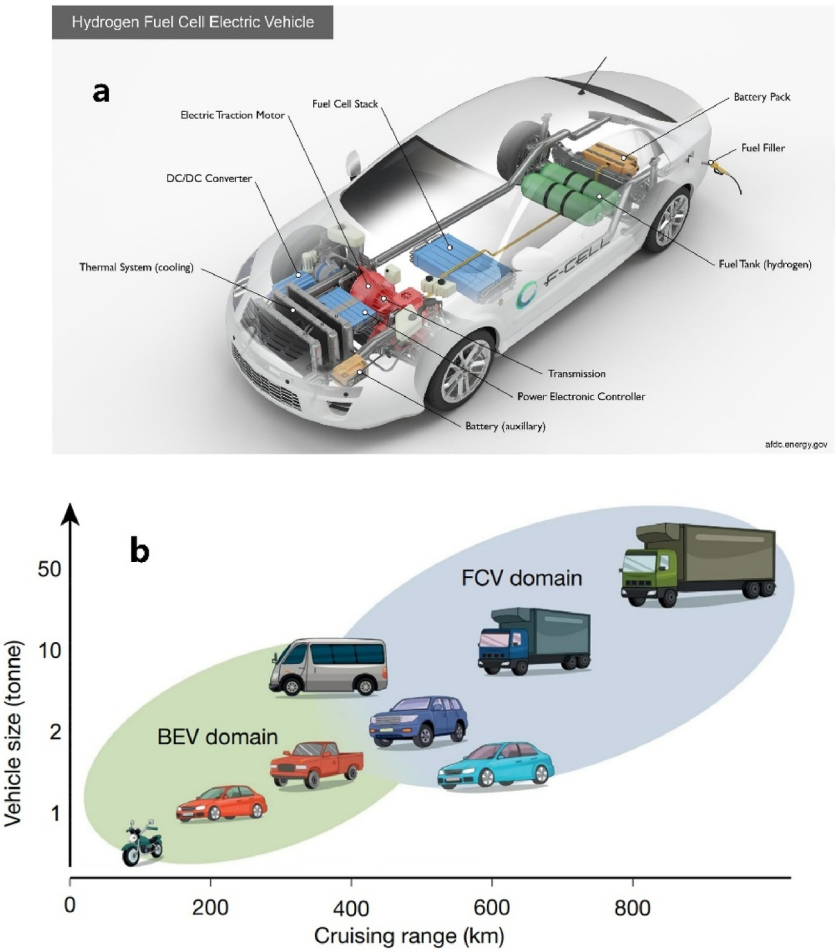

FIGURE 23 | (a) A typical structure of a fuel cell vehicle (U.S. Department of Energy, Alternative Fuels Data Center [121]). (b) The application domains of battery electric vehicles and fuel cell electric vehicles. Reproduced with permission [17], Copyright 2021, Springer Nature.

while for smaller vehicles, research efforts are centered on electrification technologies based on fuel cells. Fuel cell electric vehicles (FCEVs) are primarily powered by proton exchange membrane fuel cells (PEMFCs), which offer advantages such as high efficiency, reliable cold-start capability, and strong power output. Hydrogen is developing rapidly in the transportation sector. For example, around 814 hydrogen refueling stations were in operation globally in 2022 [119], and this number had increased to 1160 by 2024 [120]. As shown in Figure 23a, a typical FCEV consists of a fuel cell stack, a hydrogen storage system, power electronics, and a control system [121]. Although battery electric vehicles (BEVs) currently enjoy higher utilization rates and benefit from more extensively developed infrastructure, FCEVs demonstrate several advantages over BEVs, including a better energy carrier, higher energy density, shorter refueling time, lower cost and safety risks as energy density increases, and superior low-temperature performance, and Figure 23b compares the application domains of BEVs and FCEVs in the future of automotive transportation [17].

4.3 | Industrial Hydrogen

Because of its excellent reducing properties, hydrogen is widely used in various fields such as steelmaking, chemical industry, and oil refining. Currently, the refining and chemical industries account for the largest share of global hydrogen consumption, though the majority of this hydrogen is still derived from fossil fuels, that is, gray hydrogen. According to the International Energy Agency (IEA), hydrogen use in the refining sector rose to 43 Mt in 2023. Figure 24a presents the distribution of hydrogen use across different regions in the refining industry. In the industrial sector, global hydrogen demand reached 54 Mt in 2023 [122]. Around 60% of this was used for ammonia production, 30% for methanol synthesis, and the remaining 10% in the direct reduced iron (DRI) process within the iron and steel industry as shown in Figure 24b [122].

5 | Summary and Conclusions

Hydrogen, as a clean and high–energy-density secondary energy source, is widely regarded as an ideal carrier for the transition from fossil to renewable energy. Although green hydrogen production technologies are increasingly mature, large-scale, efficient, and safe hydrogen storage and transport remain challenging, leading to continued reliance on gray hydrogen. This review provides a comprehensive overview of the current status and technical bottlenecks of green hydrogen production, alongside advanced hydrogen storage and transportation technologies.

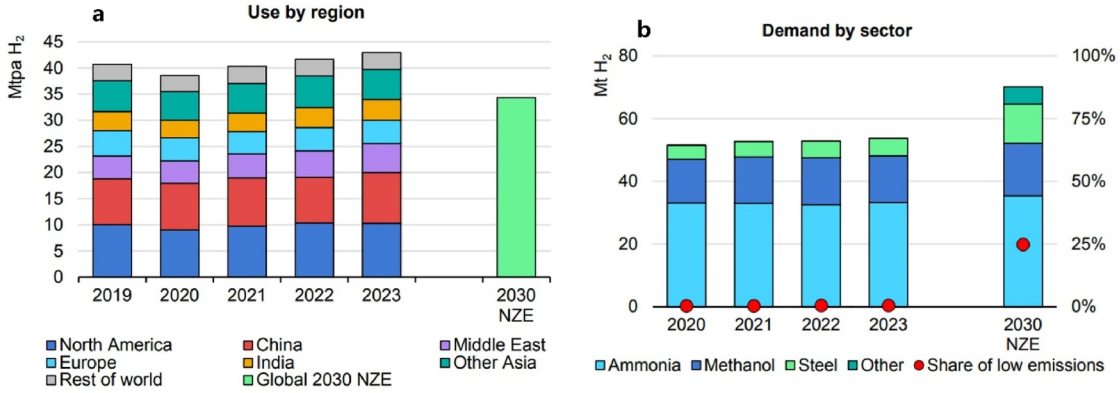

FIGURE 24 | (a) Hydrogen use by region for refining (IEA, 2024 [122]). (b) Hydrogen use in industry by subsector (IEA, 2024 [122]).

Furthermore, it assesses the decarbonization potential of green hydrogen across future transportation, industrial, and power generation sectors. The main conclusions are as follows:

1. The intermittency of renewable energy results in operational instability of electrolysis systems, high stack costs, and short service life. Therefore, future efforts should focus on improving electrolysis efficiency, reducing equipment costs, and enhancing stack durability to enable large-scale commercial deployment of green hydrogen production technologies.
2. Efficient and safe hydrogen storage and transportation remain major challenges for the large-scale development of the hydrogen industry. The development of novel hydrogen storage technologies, along with integrated solutions that combine production, storage, transportation, and utilization, will be critical for enabling large-scale and cross-regional hydrogen deployment.
3. With ongoing technological progress, deeper integration of artificial intelligence, and continuous gains in utilization efficiency, hydrogen is poised to become an increasingly vital component of future transportation, power generation, industrial applications, and large-scale energy storage systems.

Author Contributions

Xusheng Wang: writing – review and editing, writing – original draft, methodology, investigation, formal analysis, conceptualization. **Xue Yang**: funding acquisition, investigation. **Xiang Wang**: funding acquisition, investigation. **Yingyan Zhao**: investigation, writing – review and editing. **Xi Lin**: investigation, writing – review and editing. **Zhigang Hu**: investigation, writing – review and editing. **Guangqin Li**: writing – original draft, writing – review and editing. **Ruichang Xue**: writing – original draft, writing – review and editing, Investigation. **Xinwei Guan**: writing – original draft, writing – review and editing, investigation. **Baowen Zhou**: writing – review and editing, supervision, methodology, investigation. **Tianyi Ma**: writing – review and editing, supervision, methodology, investigation. **Jianxin Zou**: writing – review and editing, supervision, project administration, methodology, investigation, funding acquisition, conceptualization.

Acknowledgments

This work was supported by the National Key R&D Program of China (no. 2022YFB3803700), the National Natural Science Foundation (52401386), and the SINOPEC Research Institute of Petroleum Processing Co. Ltd. Fund (25H010102119).

Conflicts of Interest

The authors declare no conflicts of interest.

References

1. International Energy Agency, Global Energy Review (2025), https://iea.blob.core.windows.net/assets/5b169aa1-bc88-4c96-b828-aaa50406ba80/GlobalEnergyReview2025.pdf.

2. M. Chatenet, B. G. Pollet, D. R. Dekel, et al., "Water Electrolysis: From Textbook Knowledge to the Latest Scientific Strategies and Industrial Developments," *Chemical Society Reviews* 51, no. 11 (2022): 4583–4762, https://doi.org/10.1039/d0cs01079k.

3. N. Johnson, M. Liebreich, D. M. Kammen, P. Ekins, R. McKenna, and I. Staffell, "Realistic Roles for Hydrogen in the Future Energy Transition," *Nature Reviews Clean Technology* 1, no. 5 (2025): 351–371, https://doi.org/10.1038/s44359-025-00050-4.

4. National Energy Development Network, Shuangliang Group Unveils Self-Developed 5000 Nm^3/h Alkaline Electrolyzer (2024), https://www.nationalee.com/newsinfo/7738817.html.

5. S. S. Kumar and V. Himabindu, "Hydrogen Production by PEM Water Electrolysis – A Review," *Materials Science for Energy Technologies* 2, no. 3 (2019): 442–454, https://doi.org/10.1016/j.mset.2019.03.002.

6. X. Wang, J. Zou, X. Lin, et al., "Review of Research Hotspots in Green Hydrogen Production, Storage and Transportation in 2024," *Science and Technology Review* 43, no. 1 (2025): 47–61, http://www.kjdb.org/CN/lexeme/showArticleByLexeme.do?articleID=17740.

7. X. Wang, C. Tao, H. Hong, et al., "Challenges and Opportunities in Hydrogen Storage and Transportation: A Comprehensive Review," *Renewable and Sustainable Energy Reviews* 219 (2025): 115881, https://doi.org/10.1016/j.rser.2025.115881.

8. C. Gunathilake, I. Soliman, D. Panthi, et al., "A Comprehensive Review on Hydrogen Production, Storage, and Applications," *Chemical Society Reviews* 53, no. 22 (2024): 10900–10969, https://doi.org/10.1039/d3cs00731f.

9. X. Wang, L. Shao, S. Hu, et al., "A Techno-Economic Study of Photovoltaic-Solid Oxide Electrolysis Cell Coupled Magnesium Hydride-Based Hydrogen Storage and Transportation Toward Large-Scale Applications of Green Hydrogen," *Energy & Environmental Science* 17, no. 22 (2024): 8429–8456, https://doi.org/10.1039/d4ee04224g.

10. A. M. Abdalla, S. Hossain, O. B. Nisfindy, A. T. Azad, M. Dawood, and A. K. Azad, "Hydrogen Production, Storage, Transportation and Key Challenges With Applications: A Review," *Energy Conversion and*

Management 165 (2018): 602–627, https://doi.org/10.1016/j.enconman.2018.03.088.

11. Z. Hua, W. Gao, S. Chi, X. Wang, and J. Zheng, "Development Status and Challenges of High-Pressure Gaseous Hydrogen Storage Vessels and Cylinders in China," *Renewable and Sustainable Energy Reviews* 214 (2025): 115567, https://doi.org/10.1016/j.rser.2025.115567.

12. G. Leng, W. Yan, Z. Chen, et al., "Technical Challenges and Opportunities of Hydrogen Storage: A Comprehensive Review on Different Types of Underground Storage," *Journal of Energy Storage* 114 (2025): 115900, https://doi.org/10.1016/j.est.2025.115900.

13. M. Niermann, S. Drünert, M. Kaltschmitt, and K. Bonhoff, "Liquid Organic Hydrogen Carriers (LOHCs) – Techno-Economic Analysis of LOHCs in a Defined Process Chain," *Energy & Environmental Science* 12, no. 1 (2019): 290–307, https://doi.org/10.1039/c8ee02700e.

14. K. Naseem, F. Qin, F. Khalid, et al., "Essential Parts of Hydrogen Economy: Hydrogen Production, Storage, Transportation and Application," *Renewable and Sustainable Energy Reviews* 210 (2025): 115196, https://doi.org/10.1016/j.rser.2024.115196.

15. C. Anand, B. Chandraja, P. Nithiya, et al., "Green Hydrogen for a Sustainable Future: A Review of Production Methods, Innovations, and Applications," *International Journal of Hydrogen Energy* 111 (2025): 319–341, https://doi.org/10.1016/j.ijhydene.2025.02.257.

16. A. P. Zhao, S. Li, D. Xia, Y. Wang, P. J.-H. Hu, and Q. Zhang, "Hydrogen as the Nexus of Future Sustainable Transport and Energy Systems," *Nature Reviews Electrical Engineering* 2, no. 7 (2025): 447–466, https://doi.org/10.1038/s44287-025-00178-2.

17. K. Jiao, J. Xuan, Z. Bao, et al., "Designing the Next Generation of Proton-Exchange Membrane Fuel Cells," *Nature* 595, no. 7867 (2021): 361–369, https://doi.org/10.1038/s41586-021-03482-7.

18. J. Hwang, K. Maharjan, and H. Cho, "A Review of Hydrogen Utilization in Power Generation and Transportation Sectors: Achievements and Future Challenges," *International Journal of Hydrogen Energy* 48, no. 74 (2023): 28629–28648, https://doi.org/10.1016/j.ijhydene.2023.04.024.

19. L. Ge, B. Zhang, W. Huang, et al., "A Review of Hydrogen Generation, Storage, and Applications in Power System," *Journal of Energy Storage* 75 (2024): 109307, https://doi.org/10.1016/j.est.2023.109307.

20. M. Nasser, T. F. Megahed, S. Ookawara, and H. Hassan, "A Review of Water Electrolysis–Based Systems for Hydrogen Production Using Hybrid/Solar/Wind Energy Systems," *Environmental Science & Pollution Research* 29, no. 58 (2022): 86994–87018, https://doi.org/10.1007/s11356-022-23323-y.

21. J. Wang, Y. Goo, H. Kong, et al., "Non-Precious-Metal Catalysts for Alkaline Water Electrolysis: Operando Characterizations, Theoretical Calculations, and Recent Advances," *Chemical Society Reviews* 49, no. 24 (2020): 9154–9196, https://doi.org/10.1039/d0cs00575d.

22. Council on Energy, Environment and Water - Green Finance Centre, Types of Electrolysers, https://www.ceew.in/gfc/quick-reads/explains/types-of-electrolysers.

23. Hydrogen Tech World, Electrolysis Technologies and LCOH: Current State and Prospects for 2030 (2023), https://hydrogentechworld.com/electrolysis-technologies-and-lcoh-current-state-and-prospects-for-2030.

24. SENZA Hydrogen Energy and Environmental Technology, PEM Hydrogen Generator VS Alkaline Hydrogen Generator, https://senzahydrogen.com/pem-hydrogen-generator-vs-alkaline-hydrogen-generator/.

25. Sinopec, China's First 10000-Ton Photovoltaic Green Hydrogen Pilot Project Now Fully Built and Put Into Production, http://www.sinopecgroup.com/group/en/000/000/062/62515.shtml.

26. Y. Guo, P. Qi, Q. Zhang, M. Li, J. Liu, and H. Sun, "Control Strategy for Hydrogen Production System Using HTO-Based Hybrid Electrolyzers," *Energy Reports* 13 (2025): 2354–2364, https://doi.org/10.1016/j.egyr.2025.01.012.

27. S. Dash, S. K. Arjun, S. Jose, et al., "Advances in Green Hydrogen Production Through Alkaline Water Electrolysis: A Comprehensive Review," *International Journal of Hydrogen Energy* 83 (2024): 614–629, https://doi.org/10.1016/j.ijhydene.2024.08.157.

28. N. Dubouis, D. Aymé-Perrot, D. Degoulange, A. Grimaud, and H. Girault, "Alkaline Electrolyzers: Powering Industries and Overcoming Fundamental Challenges," *Joule* 8, no. 4 (2024): 883–898, https://doi.org/10.1016/j.joule.2024.02.012.

29. A. S. Emam, M. O. Hamdan, B. A. Abu-Nabah, and E. Elnajjar, "A Review on Recent Trends, Challenges, and Innovations in Alkaline Water Electrolysis," *International Journal of Hydrogen Energy* 64 (2024): 599–625, https://doi.org/10.1016/j.ijhydene.2024.03.238.

30. H. Tüysüz, "Alkaline Water Electrolysis for Green Hydrogen Production," *Accounts of Chemical Research* 57, no. 4 (2024): 558–567, https://doi.org/10.1021/acs.accounts.3c00709.

31. C. Huang, J. L. R. Torres, Y. Zong, S. You, and X. Jin, "A Review of Alkaline Electrolyzer Technology Modeling and Applications for Decision-Making Optimization in Energy Systems," *Renewable and Sustainable Energy Reviews* 224 (2025): 116005, https://doi.org/10.1016/j.rser.2025.116005.

32. Y. Kiros, M. Majari, and T. A. Nissinen, "Effect and Characterization of Dopants to Raney Nickel for Hydrogen Oxidation," *Journal of Alloys and Compounds* 360, no. 1–2 (2003): 279–285, https://doi.org/10.1016/s0925-8388(03)00346-3.

33. T. Wang, M. Wang, H. Yang, et al., "Weakening Hydrogen Adsorption on Nickel via Interstitial Nitrogen Doping Promotes Bifunctional Hydrogen Electrocatalysis in Alkaline Solution," *Energy & Environmental Science* 12 (2019): 3522–3529, https://doi.org/10.1039/c9ee01743g.

34. Y. Zuo, S. Bellani, M. Ferri, et al., "High-Performance Alkaline Water Electrolyzers Based on Ru-Perturbed Cu Nanoplatelets Cathode," *Nature Communications* 14, no. 1 (2023): 4680, https://doi.org/10.1038/s41467-023-40319-5.

35. J. Zhao, R. Urrego-Ortiz, N. Liao, F. Calle-Vallejo, and J. Luo, "Rationally Designed Ru Catalysts Supported on TiN for Highly Efficient and Stable Hydrogen Evolution in Alkaline Conditions," *Nature Communications* 15, no. 1 (2024): 6391, https://doi.org/10.1038/s41467-024-50691-5.

36. R. T. Liu, Z. L. Xu, F. M. Li, et al., "Recent Advances in Proton Exchange Membrane Water Electrolysis," *Chemical Society Reviews* 52, no. 16 (2023): 5652–5683, https://doi.org/10.1039/d2cs00681b.

37. R. Cozzolino and G. Bella, "A Review of Electrolyzer-Based Systems Providing Grid Ancillary Services: Current Status, Market, Challenges and Future Directions," *Frontiers in Energy Research* 12 (2024): 1358333, https://doi.org/10.3389/fenrg.2024.1358333.

38. F. Behrendt, "The Future of Industrial Hydrogen: Renewable Sources and Applications for the Next 15 Years," *Clean Energy* 9, no. 1 (2025): 3–8, https://doi.org/10.1093/ce/zkae103.

39. P. Mottaghizadeh, F. Jabbari, and J. Brouwer, "Integrated Solid Oxide Fuel Cell, Solar PV, and Battery Storage System to Achieve Zero Net Energy Residential Nanogrid in California," *Applied Energy* 323 (2022): 119577, https://doi.org/10.1016/j.apenergy.2022.119577.

40. H. B. Tao, H. Liu, K. Lao, et al., "The Gap Between Academic Research on Proton Exchange Membrane Water Electrolysers and Industrial Demands," *Nature Nanotechnology* 19, no. 8 (2024): 1074–1076, https://doi.org/10.1038/s41565-024-01699-x.

41. C. Su, Z. Chen, Z. Wu, et al., "Experimental and Numerical Study of Thermal Coupling on Catalyst-Coated Membrane for Proton Exchange Membrane Water Electrolyzer," *Applied Energy* 357 (2024): 122442, https://doi.org/10.1016/j.apenergy.2023.122442.

42. S. Wang, L. Liu, H. Xin, and C. Ling, "Toward a Stable and Active Catalyst for Proton-Exchange Membrane Water Electrolysis," *Chem Catalysis* 4, no. 1 (2024): 100869, https://doi.org/10.1016/j.checat.2023.100869.

43. J. Tang, X. Liu, X. Xiong, et al., "Ruthenium Single-Atom Modulated Protonated Iridium Oxide for Acidic Water Oxidation in Proton Exchange Membrane Electrolysers," *Advanced Materials* 36, no. 41 (2024): e2407394, https://doi.org/10.1002/adma.202407394.

44. Y. Wang, Z. Zhao, X. Liang, et al., "Supported IrO_2 Nanocatalyst With Multilayered Structure for Proton Exchange Membrane Water Electrolysis," *Advanced Materials* 36, no. 39 (2024): e2407717, https://doi.org/10.1002/adma.202407717.

45. Y. Shen, X. L. Zhang, M. R. Qu, et al., "Cr Dopant Mediates Hydroxyl Spillover on RuO(2) for high-efficiency Proton Exchange Membrane Electrolysis," *Nature Communications* 15, no. 1 (2024): 7861, https://doi.org/10.1038/s41467-024-51871-z.

46. EVE Energy, EVE Hydrogen Dispatches China's First AEM Electrolysis System to Hubei Province, https://www.evebattery.com/news-824.

47. X. Jin, S. You, M. Petersen, et al., "Exploring Commercial Water Electrolyser Systems: A Data-Based Analysis of Product Characteristics," *Clean Energy* 8, no. 1 (2024): 126–133, https://doi.org/10.1093/ce/zkad072.

48. S. Shaik, J. Kundu, Y. Yuan, et al., "Recent Progress and Perspective in Pure Water-Fed Anion Exchange Membrane Water Electrolyzers," *Advanced Energy Materials* 14, no. 35 (2024): 2401956, https://doi.org/10.1002/aenm.202401956.

49. Z. Li, G. Lin, L. Wang, et al., "Seed-Assisted Formation of NiFe Anode Catalysts for Anion Exchange Membrane Water Electrolysis at Industrial-Scale Current Density," *Nature Catalysis* 7, no. 8 (2024): 944–952, https://doi.org/10.1038/s41929-024-01209-1.

50. L. Yin, R. Ren, L. He, et al., "Stable Anion Exchange Membrane Bearing Quinuclidinium for High-Performance Water Electrolysis," *Angewandte Chemie International Edition in English* 63, no. 19 (2024): e202400764, https://doi.org/10.1002/ange.202400764.

51. M. Götz, J. Lefebvre, F. Mörs, et al., "Renewable Power-to-Gas: A Technological and Economic Review," *Renewable Energy* 85 (2016): 1371–1390, https://doi.org/10.1016/j.renene.2015.07.066.

52. I.-O. Karittha, V. Nuttawut, S. Dang, Y. Patcharavorachot, and A. Arpornwichanop, "Flowsheet-Based Model and Exergy Analysis of Solid Oxide Electrolysis Cells for Clean Hydrogen Production," *Journal of Cleaner Production* 170 (2018): 1–13, https://doi.org/10.1016/j.jclepro.2017.09.127.

53. A. Hauch, R. Küngas, P. Blennow, et al., "Recent Advances in Solid Oxide Cell Technology for Electrolysis," *Science* 370, no. 6513 (2020): 6118, https://doi.org/10.1126/science.aba6118.

54. Hydrogen Tech World, GrInHy2.0 Project Completed With Record Production Rates, https://hydrogentechworld.com/grinhy2-0-project-completed-with-record-production-rates#:~:text=GrInHy2.,hydrogen%20grid%20of%20Salzgitter%20Flachstahl.

55. Power Engineering, Mitsubishi Heavy Industries Begins Testing Solid Oxide Electrolyzer Cell for Hydrogen Production (2024), https://www.power-eng.com/.

56. Y. Wang, W. Li, L. Ma, and X. Liu, "Degradation of Solid Oxide Electrolysis Cells: Phenomena, Mechanisms, and Emerging Mitigation Strategies—A Review," *Journal of Materials Science and Technology* 55 (2020): 35–55, https://doi.org/10.1016/j.jmst.2019.07.026.

57. S. E. Wolf, F. E. Winterhalder, V. Vibhu, et al., "Solid Oxide Electrolysis Cells-Current Material Development and Industrial Application," *Journal of Materials Chemistry A* 11, no. 34 (2023): 17977–18028, https://doi.org/10.1039/d3ta02161k.

58. H. Shimada, T. Yamaguchi, H. Kishimoto, et al., "Nanocomposite Electrodes for High Current Density over 3 A cm^{-2} in Solid Oxide Electrolysis Cells," *Nature Communications* 10, no. 1 (2019): 5432, https://doi.org/10.1038/s41467-019-13426-5.

59. Y. Guo, S. Wang, R. Li, et al., "In Situ Exsolved CoFe Alloy Nanoparticles for Stable Anodic Methane Reforming in Solid Oxide Electrolysis Cells," *Joule* 8, no. 7 (2024): 2016–2032, https://doi.org/10.1016/j.joule.2024.04.009.

60. S. Josef, P. Hendrik, and B. Annabelle, "Solid Oxide Electrolyser Cell Testing up to the Above 30,000 H Time Range," *ECS Transactions* 97, no. 7 (2020): 553–563, https://doi.org/10.1149/09707.0553ecst.

61. L. A. Jolaoso, I. T. Bello, O. A. Ojelade, A. Yousuf, C. Duan, and P. Kazempoor, "Operational and scaling-up Barriers of SOEC and Mitigation Strategies to Boost H2 production- a Comprehensive Review," *International Journal of Hydrogen Energy* 48, no. 85 (2023): 33017–33041, https://doi.org/10.1016/j.ijhydene.2023.05.077.

62. K. Takanabe, "Photocatalytic Water Splitting: Quantitative Approaches Toward Photocatalyst by Design," *ACS Catalysis* 7, no. 11 (2017): 8006–8022, https://doi.org/10.1021/acscatal.7b02662.

63. A. Fujishima and K. Honda, "Electrochemical Photolysis of Water at a Semiconductor Electrode," *Nature* 238, no. 5358 (1972): 37–38, https://doi.org/10.1038/238037a0.

64. H. Nishiyama, T. Yamada, M. Nakabayashi, et al., "Photocatalytic Solar Hydrogen Production From Water on a 100-m^2 Scale," *Nature* 598, no. 7880 (2021): 304–307, https://doi.org/10.1038/s41586-021-03907-3.

65. D. Wang, A. Pierre, G. M. Kibria, et al., "Wafer-Level Photocatalytic Water Splitting on GaN Nanowire Arrays Grown by Molecular Beam Epitaxy," *Nano Letters* 11, no. 6 (2011): 2353–2357, https://doi.org/10.1021/nl2006802.

66. P. Zhou, A. I. Navid, Y. Ma, et al., "Solar-To-Hydrogen Efficiency of More Than 9% in Photocatalytic Water Splitting," *Nature* 613, no. 7942 (2023): 66–70, https://doi.org/10.1038/s41586-022-05399-1.

67. S. M. Nasir, Y. Zhao, H. Ye, et al., "Efficient Hole Extraction and *OH Alleviation by Pd Nanoparticles on GaN Nanowires in Seawater for Solar-Driven H_2 and H_2O_2 Generation," *Angewandte Chemie International Edition* 64, no. 10 (2025): e202420796, https://doi.org/10.1002/anie.202420796.

68. J. Yu, J. Huang, R. Li, Y. Li, G. Liu, and X. Xu, "Fluorine-Expedited Nitridation of Layered Perovskite Sr_2TiO_4 for Visible-Light-Driven Photocatalytic Overall Water Splitting," *Nature Communications* 16, no. 1 (2025): 361, https://doi.org/10.1038/s41467-024-55748-z.

69. J. Xiao, M. Nakabayashi, T. Hisatomi, et al., "Sub-50 Nm Perovskite-Type Tantalum-Based Oxynitride Single Crystals With Enhanced Photoactivity for Water Splitting," *Nature Communications* 14, no. 1 (2023): 8030, https://doi.org/10.1038/s41467-023-43838-3.

70. J. D. Qu, Y. Wang, T. T. Sun, et al., "Engineering Covalent Organic Frameworks for Photocatalytic Overall Water Vapor Splitting," *Angewandte Chemie International Edition* 64, no. 22 (2025): e202502821, https://doi.org/10.1002/anie.202502821.

71. R. C. Shen, C. Huang, L. Hao, et al., "Ground-State Charge Transfer in Single-Molecule Junctions Covalent Organic Frameworks for Boosting Photocatalytic Hydrogen Evolution," *Nature Communications* 16, no. 1 (2025): 2457, https://doi.org/10.1038/s41467-025-57662-4.

72. K. Sun, Y. Huang, F. S. Sun, et al., "Dynamic Structural Twist in Metal-Organic Frameworks Enhances Solar Overall Water Splitting," *Nature Chemistry* 16, no. 10 (2024): 1638–1646, https://doi.org/10.1038/s41557-024-01599-6.

73. T. Hisatomi and K. Domen, "Reaction Systems for Solar Hydrogen Production via Water Splitting With Particulate Semiconductor Photocatalysts," *Nature Catalysis* 2, no. 5 (2019): 387–399, https://doi.org/10.1038/s41929-019-0242-6.

74. B. Weng, M. Y. Qi, C. Han, Zi-R. Tang, and Yi-J. Xu, "Photocorrosion Inhibition of Semiconductor-Based Photocatalysts: Basic Principle, Current Development, and Future Perspective," *ACS Catalysis* 9, no. 5 (2019): 4642–4687, https://doi.org/10.1021/acscatal.9b00313.

75. Z. W. Seh, J. Kibsgaard, C. F. Dickens, I. B. Chorkendorff, J. K. Nørskov, and T. F. Jaramillo, "Combining Theory and Experiment in Electrocatalysis: Insights Into Materials Design," *Science* 355, no. 6321 (2017): eaad4998, https://doi.org/10.1126/science.aad4998.

76. H. Tada, T. Mitsui, T. Kiyonaga, T. Akita, and K. Tanaka, "All-Solid-State Z-Scheme in CdS–Au–TiO_2 Three-Component Nanojunction System," *Nature Materials* 5, no. 10 (2006): 782–786, https://doi.org/10.1038/nmat1734.

77. X. Chen, L. Liu, P. Y. Yu, and S. S. Mao, "Increasing Solar Absorption for Photocatalysis With Black Hydrogenated Titanium Dioxide Nanocrystals," *Science* 331, no. 6018 (2011): 746–750, https://doi.org/10.1126/science.1200448.

78. K. Maeda and K. Domen, "Photocatalytic Water Splitting: Recent Progress and Future Challenges," *Journal of Physical Chemistry Letters* 1, no. 18 (2010): 2655–2661, https://doi.org/10.1021/jz1007966.

79. G. Liu, H. G. Yang, J. Pan, Y. Q. Yang, G. Q. M. Lu, and H.-M. Cheng, "Titanium Dioxide Crystals With Tailored Facets," *Chemical Reviews* 114, no. 19 (2014): 9559–9612, https://doi.org/10.1021/cr400621z.

80. X. Chen, L. Liu, Z. Liu, et al., "Properties of Disorder-Engineered Black Titanium Dioxide Nanoparticles Through Hydrogenation," *Scientific Reports* 3, no. 1 (2013): 1510, https://doi.org/10.1038/srep01510.

81. A. Solanki and S. H. Turren-Cruz, "Hybrid Perovskite Photocatalysis for Energy Harvesting and Energy Saving," in *Nano-Catalysts for Energy Applications* (Taylor & Francis Group, 2021).

82. D. Kim, K. K. Sakimoto, D. Hong, and P. Yang, "Artificial Photosynthesis for Sustainable Fuel and Chemical Production," *Angewandte Chemie International Edition* 54, no. 11 (2015): 3259–3266, https://doi.org/10.1002/anie.201409116.

83. C. Mu, C. Lv, X. Meng, J. Sun, Z. Tong, and K. Huang, "In Situ Characterization Techniques Applied in Photocatalysis: A Review," *Advanced Materials Interfaces* 10, no. 3 (2023): 2201842, https://doi.org/10.1002/admi.202201842.

84. E. Boateng and A. Chen, "Recent Advances in Nanomaterial-Based Solid-State Hydrogen Storage," *Materials Today Advances* 6 (2020): 100022, https://doi.org/10.1016/j.mtadv.2019.100022.

85. B. Ghorbani, S. Zendehboudi, N. M. C. Saady, and M. B. Dusseault, "Hydrogen Storage in North America: Status, Prospects, and Challenges," *Journal of Environmental Chemical Engineering* 11, no. 3 (2023): 109957, https://doi.org/10.1016/j.jece.2023.109957.

86. U.S. Department of Energy, Materials-Based Hydrogen Storage, https://www.energy.gov/eere/fuelcells/materials-based-hydrogen-storage.

87. B. Zohuri, "Hydrogen Energy Technology, Renewable Source of Energy," in *Hybrid Energy Systems* (Springer, 2018), https://doi.org/10.1007/978-3-319-70721-1_5.

88. L. Ren, Y. Li, N. Zhang, et al., "Nanostructuring of Mg-Based Hydrogen Storage Materials: Recent Advances for Promoting Key Applications," *Nano-Micro Letters* 15, no. 1 (2023): 93, https://doi.org/10.1007/s40820-023-01041-5.

89. E. M. Dematteis, M. B. Amdisen, T. Autrey, et al., "Hydrogen Storage in Complex Hydrides: Past Activities and New Trends," *Progress in Energy* 4, no. 3 (2022): 032009, https://doi.org/10.1088/2516-1083/ac7499.

90. L. Zi, Y. Li, K. Huang, et al., "Balancing Nucleation and Growth Kinetics Enables Fully-Coordinated Acetic Acid-Tethered Metal–Organic Frameworks for Technoeconomic-Viable Hydrogen Storage," *Advanced Energy Materials* (2025): e03259, https://doi.org/10.1002/aenm.202503259.

91. A. Gupta, G. V. Baron, P. Perreault, et al., "Hydrogen Clathrates: Next Generation Hydrogen Storage Materials," *Energy Storage Materials* 41 (2021): 69–107, https://doi.org/10.1016/j.ensm.2021.05.044.

92. X. Zhang, S. Ju, C. Li, et al., "Atomic Reconstruction for Realizing Stable Solar-Driven Reversible Hydrogen Storage of Magnesium Hydride," *Nature Communications* 15, no. 1 (2024): 2815, https://doi.org/10.1038/s41467-024-47077-y.

93. T. Huang, Y. Zhao, B. Wang, et al., "MOFs Derived Ni-Mn Bimetal Nano-Catalysts With Enhanced Hydrogen Pump Effect for Boosting Hydrogen Sorption Performance of MgH_2," *Journal of Magnesium and Alloys* (2024), https://doi.org/10.1016/j.jma.2024.11.008.

94. HyReachX, http://www.zkxdnewenergy.com/info/76187.html.

95. Hydrexia, https://www.hydrexia.com/products/storage_transport.

96. L. A. Lesmana and M. Aziz, "Strategic Integration of Metamaterials Properties and Topology Optimization of Gyroid Metal Hydride Reactor for High-Density Hydrogen Storage," *Energy* 308 (2024): 133018, https://doi.org/10.1016/j.energy.2024.133018.

97. P. C. Rao and M. Yoon, "Potential Liquid-Organic Hydrogen Carrier (LOHC) Systems: A Review on Recent Progress," *Energies* 13, no. 22 (2020): 6040, https://doi.org/10.3390/en13226040.

98. Fuel Cells Works, Hydrogen Transportation in the Form of MCH by Chemical Tanker (2022), https://fuelcellsworks.com/%20news/hydrogen-transportation-in-the-form-of-mch-by-chemical-tanker.

99. Hydrogenious LOHC Technologies, https://hydrogenious.net/.

100. M. Dai, Y. Qin, L. Chen, and X. Chen, "A Review of Reversible Hydrogenation and Dehydrogenation Catalysts for Liquid Organic Hydrogen Carriers," *Catalysis Science and Technology* 15, no. 8 (2025): 2440–2449, https://doi.org/10.1039/d4cy01483a.

101. A. Ali and M. N. Shaikh, "Recent Developments in Catalyst Design for Liquid Organic Hydrogen Carriers: Bridging the Gap to Affordable Hydrogen Storage," *International Journal of Hydrogen Energy* 78 (2024): 1–21, https://doi.org/10.1016/j.ijhydene.2024.06.240.

102. L. Zhu, Y. Jiang, J. Zheng, et al., "Ultrafine Nanoparticle-Supported Ru Nanoclusters With Ultrahigh Catalytic Activity," *Small* 11, no. 34 (2015): 4385–4393, https://doi.org/10.1002/smll.201500654.

103. Z. Jiang, X. Gong, B. Wang, Z. Wu, and T. Fang, "A Experimental Study on the Dehydrogenation Performance of dodecahydro-*N*-Ethylcarbazole on M/TiO_2 Catalysts," *International Journal of Hydrogen Energy* 44, no. 5 (2019): 2951–2959, https://doi.org/10.1016/j.ijhydene.2018.11.236.

104. M. Schörner, T. Solymosi, T. Razcka, et al., "Inductively Heatable Catalytic Materials for the Dehydrogenation of the Liquid Organic Hydrogen Carrier (LOHC) Perhydro Dibenzyltoluene," *Catalysis Science and Technology* 14, no. 16 (2024): 4450–4457, https://doi.org/10.1039/d4cy00272e.

105. X. Wang, M. Gao, A. P. R. Harrison, et al., "A Green Ammonia Utilization Pathway: Integrated Ammonia-Solid Oxide Fuel Cell Systems for Efficient Power Generation," *EnergyChem* 7, no. 5 (2025): 100167, https://doi.org/10.1016/j.enchem.2025.100167.

106. S. Chatterje, R. K. Parsapur, and K.-W. Huang, "Limitations of Ammonia as a Hydrogen Energy Carrier for the Transportation Sector," *ACS Energy Letters* 6, no. 12 (2021): 4390–4394, https://doi.org/10.1021/acsenergylett.1c02189.

107. Chang, F., I. Tezsevin, J. W. Rijk, et al., "Potassium Hydride-Intercalated Graphite as an Efficient Heterogeneous Catalyst for Ammonia Synthesis," *Nature Catalysis* 5, no. 3 (2022): 222–230, https://doi.org/10.1038/s41929-022-00754-x.

108. H. Tabassu, S. Mukherjee, J. Chen, et al., "Hydrogen Generation via Ammonia Decomposition on Highly Efficient and Stable Ru-Free Catalysts: Approaching Complete Conversion at 450°C," *Energy &*

Environmental Science 15, no. 10 (2022): 4190–4200, https://doi.org/10.1039/d1ee03730g.

109. C. Hakanda, H. S. Pramono, and M. Aziz, "Conversion of Municipal Solid Waste to Hydrogen and Its Storage to Methanol," *Sustainable Energy Technologies and Assessments* 51 (2022): 101968, https://doi.org/10.1016/j.seta.2022.101968.

110. C. Su, H. Wei, Z. Wang, H. Ayed, A. Mouldi, and A. A. Shayesteh, "Economic Accounting and High-Tech Strategy for Sustainable Production: A Case Study of Methanol Production From CO_2 Hydrogenation," *International Journal of Hydrogen Energy* 47, no. 62 (2022): 25929–25944, https://doi.org/10.1016/j.ijhydene.2022.01.124.

111. I. Ganesh, "Conversion of Carbon Dioxide into Methanol – A Potential Liquid Fuel: Fundamental Challenges and Opportunities (A Review)," *Renewable and Sustainable Energy Reviews* 31 (2014): 221–257, https://doi.org/10.1016/j.rser.2013.11.045.

112. Hydrogen Council, Hydrogen for Net-Zero A Critical Cost-Competitive Energy Vector (November 2021), https://hydrogencouncil.com/wp-content/uploads/2021/11/Hydrogen-for-Net-Zero.pdf.

113. H. Nagamoto, *Fuel Cells: Electrochemical Reactions* (Encyclopedia of Materials: Science and Technology, 2001), 3359–3367, https://doi.org/10.1016/B0-08-043152-6/00600-8.

114. Office of Energy Efficiency & Renewable Energy, Comparison of Fuel Cell Technologies, https://www.energy.gov/eere/fuelcells/comparison-fuel-cell-technologies.

115. S. N. Fereshteh and S. Bengt, "Review of Exergy and Energy Analysis of Fuel Cells," *International Journal of Hydrogen Energy* 48, no. 84 (2023): 32875–32942, https://doi.org/10.1016/j.ijhydene.2023.05.052.

116. G. Seyedehhoma, V. Maria, I. A. G. Wilson, and P. Styring, "Sustainable Ammonia Production Processes," *Frontiers in Energy Research* 9 (2021): 580808, https://doi.org/10.3389/fenrg.2021.580808.

117. C. Bao, Y. Wang, D. Feng, Z. Jiang, and X. Zhang, "Macroscopic Modeling of Solid Oxide Fuel Cell (SOFC) and Model-Based Control of SOFC and Gas Turbine Hybrid System," *Progress in Energy and Combustion Science* 66 (2018): 83–140, https://doi.org/10.1016/j.pecs.2017.12.002.

118. H. Zhou, J. Xue, H. Gao, and N. Ma, "Hydrogen-Fueled Gas Turbines in Future Energy System," *International Journal of Hydrogen Energy* 64 (2024): 569–582, https://doi.org/10.1016/j.ijhydene.2024.03.327.

119. H. Sahin, "Hydrogen Refueling of a Fuel Cell Electric Vehicle," *International Journal of Hydrogen Energy* 75 (2024): 604–612, https://doi.org/10.1016/j.ijhydene.2024.04.021.

120. Fuel Cells Works, Milestone Reached: Over 1,000 Hydrogen Refuelling Stations in Oper-Ation Worldwide in 2024, https://fuelcellsworks.com/2025/02/12/h2/milestone-reached-over-1-000-hydrogen-refuelling-stations-in-oper-ation-worldwide-in-2024#google_vignette.

121. U.S. Department of Energy, Alternative Fuels Data Center, How Do Fuel Cell Electric Vehicles Work Using Hydrogen?, https://afdc.energy.gov/vehicles/how-do-fuel-cell-electric-cars-work.

122. International Energy Agency, Global Hydrogen Review 2024, https://iea.blob.core.windows.net/assets/89c1e382-dc59-46ca-aa47-9f7d41531ab5/GlobalHydrogenReview2024.pdf.